



Universiteit  
Leiden  
The Netherlands

## Tissue-resident memory CD8(+)T cells shape local and systemic secondary T cell responses

Behr, F.M.; Parga-Vidal, L.; Kragten, N.A.M.; Dam, T.J.P. van; Wesselink, T.H.; Sheridan, B.S.; ... ; Gisbergen, K.P.J.M. van

### Citation

Behr, F. M., Parga-Vidal, L., Kragten, N. A. M., Dam, T. J. P. van, Wesselink, T. H., Sheridan, B. S., ... Gisbergen, K. P. J. M. van. (2020). Tissue-resident memory CD8(+)T cells shape local and systemic secondary T cell responses. *Nature Immunology*, 21(9), 1070-1081. doi:10.1038/s41590-020-0723-4

Version: Publisher's Version  
License: [Creative Commons CC BY 4.0 license](#)  
Downloaded from: <https://hdl.handle.net/1887/3182688>

**Note:** To cite this publication please use the final published version (if applicable).



# Tissue-resident memory CD8<sup>+</sup> T cells shape local and systemic secondary T cell responses

Felix M. Behr <sup>1,2,6</sup>, Loreto Parga-Vidal<sup>1,6</sup>, Natasja A. M. Kragten<sup>1</sup>, Teunis J. P. van Dam<sup>1,3</sup>, Thomas H. Wesselink <sup>1</sup>, Brian S. Sheridan<sup>4</sup>, Ramon Arens <sup>5</sup>, Rene A. W. van Lier <sup>1</sup>, Regina Stark <sup>1,2</sup> and Klaas P. J. M. van Gisbergen <sup>1,2</sup> ✉

**Tissue-resident memory CD8<sup>+</sup> T cells (T<sub>RM</sub> cells) are crucial in protecting against reinventing pathogens, but the impact of reinfection on their tissue confinement and contribution to recall responses is unclear. We developed a unique lineage tracer mouse model exploiting the T<sub>RM</sub>-defining transcription factor homolog of Blimp-1 in T cells (Hobit) to fate map the T<sub>RM</sub> progeny in secondary responses. After reinfection, a sizeable fraction of secondary memory T cells in the circulation developed downstream of T<sub>RM</sub> cells. These tissue-experienced ex-T<sub>RM</sub> cells shared phenotypic properties with the effector memory T cell population but were transcriptionally and functionally distinct from other secondary effector memory T cell cells. Adoptive transfer experiments of T<sub>RM</sub> cells corroborated their potential to form circulating effector and memory cells during recall responses. Moreover, specific ablation of primary T<sub>RM</sub> cell populations substantially impaired the secondary T cell response, both locally and systemically. Thus, T<sub>RM</sub> cells retain developmental plasticity and shape both local and systemic T cell responses on reinfection.**

Immune protection against intracellular pathogens is mediated by distinct subsets of CD8<sup>+</sup> T cells. Upon antigen encounter in secondary lymphoid organs (SLOs), pathogen-specific naïve CD8<sup>+</sup> T cells undergo rapid expansion and differentiate into effector and long-lived memory CD8<sup>+</sup> T cells. Memory CD8<sup>+</sup> T cells protect against subsequent reinfection and consist of subsets with distinct migratory and functional properties<sup>1,2</sup>. Similar to their naïve counterparts, central memory T cells (T<sub>CM</sub> cells) maintain the capacity to survey SLOs via the expression of lymph node homing molecules, such as CCR7 and L-selectin (CD62L), and mount strong proliferative responses on reinfection<sup>3</sup>. Effector memory cells (T<sub>EM</sub> cells) primarily patrol regions outside lymph nodes, including nonlymphoid tissues<sup>4</sup>, and are poised for rapid execution of effector functions, but not proliferative expansion<sup>5–7</sup>. In contrast to these circulating memory T cells, T<sub>RM</sub> cells are absent from the blood and persist in peripheral tissues, where they provide enhanced protection against subsequent infections.

Next to their constrained anatomical localization, T<sub>RM</sub> cells are characterized by a unique gene expression program that includes expression of the transcription factor Hobit (ZNF683) (refs. <sup>8,9</sup>). Together with its homolog Blimp-1, Hobit mediates T<sub>RM</sub> cell formation in several tissues<sup>9</sup>. Both transcription factors cooperate in controlling tissue retention by downregulating tissue exit pathways, including *Ccr7* and *S1pr1*, and suppressing transcription factors that regulate circulating memory T cells, for example, Krueppel-like factor 2 (Klf2) and transcription factor 7 (Tcf7) (ref. <sup>9</sup>). Immunosurveillance of nonlymphoid tissues in the absence of inflammation is predominantly executed by local T<sub>RM</sub> cells rather than circulating memory T cells<sup>10</sup>. Following pathogen reencounter, T<sub>RM</sub> cells promptly engage effector functions, including the

production of pro-inflammatory cytokines, thus providing local immunosurveillance and rapid protection against reinfections<sup>11,12</sup>. Moreover, T<sub>RM</sub> cells proliferate in situ on antigen encounter and generate a secondary pool of T<sub>RM</sub> cells<sup>13,14</sup>. However, little is known regarding the contribution of T<sub>RM</sub> cells to secondary responses beyond their local tissue. Recent evidence suggests that T<sub>RM</sub> cells can exit nonlymphoid tissues on local reactivation and yield secondary T<sub>RM</sub> cells in lymph nodes draining their tissue of residence<sup>15</sup>. It is unclear whether reinfections also lead to the recruitment of reactivated T<sub>RM</sub> cells into the pool of circulating T cells.

Successive infections not only drive the expansion of the memory T cell compartment, but also qualitatively shape the circulating memory T cell population<sup>16–20</sup>. Repeated antigen exposure biases the circulating memory pool toward a T<sub>EM</sub> phenotype, as indicated by reduced expression of CD62L, elevated expression of killer cell lectin-like receptor subfamily G member 1 (KLRG1) and increased cytotoxic activity<sup>17,18,20,21</sup>. Moreover, secondary memory T cells provide enhanced protection against acute infection with intracellular pathogens, which is potentially mediated through persistent cytotoxic capacity<sup>18,19</sup>. How secondary T<sub>EM</sub> cells with different properties arise and the factors and cell populations driving these adaptations are unclear. Reactivated T<sub>CM</sub> cells can give rise to offspring with a T<sub>EM</sub> phenotype<sup>22,23</sup>, but it is not well understood to which extent this differentiation drives the accumulation of T<sub>EM</sub> cells after reinfection. Importantly, the contribution of T<sub>RM</sub> cells to local and systemic recall responses and their differentiation potential into circulating memory T cell subsets is unclear.

To investigate secondary T<sub>RM</sub> cell responses, we developed a reporter system exploiting the T<sub>RM</sub>-restricted transcription factor Hobit to visualize T<sub>RM</sub> cells and fate map their progeny on

<sup>1</sup>Department of Hematopoiesis, Sanquin Research and Landsteiner Laboratory, Amsterdam UMC, University of Amsterdam, Amsterdam, the Netherlands.

<sup>2</sup>Department of Experimental Immunology, Amsterdam UMC, University of Amsterdam, Amsterdam, the Netherlands. <sup>3</sup>Department of Molecular and Cellular Hemostasis, Sanquin Research and Landsteiner Laboratory, Amsterdam UMC, University of Amsterdam, Amsterdam, the Netherlands.

<sup>4</sup>Department of Microbiology and Immunology, Renaissance School of Medicine, Stony Brook University, Stony Brook, NY, USA. <sup>5</sup>Department of Immunohematology and Blood Transfusion, Leiden University Medical Center, Leiden, the Netherlands. <sup>6</sup>These authors contributed equally: Felix M. Behr, Loreto Parga-Vidal. ✉e-mail: [k.vangisbergen@sanquin.nl](mailto:k.vangisbergen@sanquin.nl)

reinfection. Using this system in combination with two distinct complementary models, we show that reinfection induces local expansion of  $T_{RM}$  cells in peripheral tissues, accumulation of secondary  $T_{RM}$  cells in draining lymph nodes and development of a large fraction of secondary memory T cells in the circulation downstream of  $T_{RM}$  cells. These circulating ex- $T_{RM}$  cells phenotypically resemble  $T_{EM}$  cells, with distinct transcriptional and functional properties. Taken together, we demonstrate that  $T_{RM}$  cells substantially contribute to secondary responses beyond their tissue of origin.

## Results

**Hobit identifies  $T_{RM}$  cells across tissues.** Analysis of  $T_{RM}$  cells *in vivo* primarily relies on phenotypic surface markers, which may be subject to change on  $T_{RM}$  reactivation<sup>24</sup>. We have previously demonstrated that the transcription factor Hobit is selectively expressed by  $T_{RM}$  cells, but not by circulating memory T cells<sup>9</sup>, suggesting that Hobit can be exploited to specifically visualize and manipulate  $T_{RM}$  cells. Therefore, we developed Hobit reporter mice containing a reporter cassette encoding for the fluorescent protein tdTomato, the Cre recombinase and the diphtheria toxin receptor (DTR) in the *Hobit* locus (Fig. 1a). Hobit reporter mice were crossed with T cell receptor (TCR) transgenic OT-I mice, whose CD8<sup>+</sup> T cells recognize the ovalbumin (OVA)-derived peptide SIINFEKL, to enable the study of antigen-specific T cell responses developing after oral infection with *Listeria monocytogenes*-expressing OVA (Lm-OVA). At >30 d post infection, adoptively transferred naïve Hobit reporter OT-I T cells differentiated into circulating CD62L<sup>+</sup>CD69<sup>-</sup>  $T_{CM}$  and CD62L<sup>-</sup>CD69<sup>-</sup>  $T_{EM}$  cells in the spleen, mesenteric lymph nodes (MLNs) and liver (Fig. 1b,c). Furthermore, CD62L<sup>-</sup>CD69<sup>+</sup>  $T_{RM}$  cells were formed in the liver, and the small intestine lamina propria (SI-LPL) and intraepithelial lymphocyte (SI-IEL) compartments. In agreement with previous findings<sup>25</sup>, the intestinal compartments almost exclusively harbored OT-I T cells with a  $T_{RM}$  phenotype. The transgene tdTomato (reporting Hobit) was strongly and uniformly expressed in  $T_{RM}$  cells, but nearly absent in  $T_{CM}$  and  $T_{EM}$  cells (Fig. 1d,e). Hobit messenger RNA was detected in tdTomato<sup>+</sup>  $T_{RM}$  cells, but not in tdTomato<sup>-</sup>  $T_{EM}$  or  $T_{CM}$  cells, confirming the accuracy of the Hobit reporter system (Extended Data Fig. 1a–c). Thus, tdTomato expression in Hobit reporter mice specifically identified  $T_{RM}$  cells arising in the liver and small intestine after oral Lm-OVA infection. These findings suggest that the Hobit reporter system allows for the direct visualization and genetic manipulation of  $T_{RM}$  cells.

**$T_{RM}$  cells expand locally and in draining lymph nodes on reinfection.** Next, we investigated the impact of pathogen reencounter on the dynamics of Hobit expression in intestinal  $T_{RM}$  cells. Mice harboring memory populations of Hobit reporter OT-I T cells after a primary oral Lm-OVA infection were rechallenged with Lm-OVA. Intestinal OT-I T cells expanded strongly after rechallenge and were maintained at elevated numbers compared to the primary memory phase (Fig. 2a,b). The majority of intestinal OT-I T cells maintained coexpression of CD69 and Hobit (tdTomato) in the effector (3 and 8 d) and memory phase (>30 d) after rechallenge (Fig. 2a). While a substantial fraction of intestinal OT-I T cells did not express CD69 and Hobit in the effector phase on day 8 after reinfection, the vast majority of both primary and secondary memory OT-I T cells exhibited coexpression of both molecules. These findings suggest that Hobit-expressing  $T_{RM}$  cells accumulate locally within the small intestine after reinfection.

MLNs, which drain intestinal infection sites, did not contain detectable numbers of Hobit-expressing OT-I T cells after primary infection (Fig. 2a). In contrast, we observed CD69<sup>lo</sup>Hobit<sup>+</sup> OT-I T cells in MLNs in the effector phase on day 8 after reinfection. Hobit<sup>+</sup> OT-I T cells were retained in MLNs and upregulated CD69 expression in the secondary memory phase (Fig. 2a,b). Taken

together, these data indicate that reinfection at intestinal sites drives local expansion of  $T_{RM}$  cells and the emergence of  $T_{RM}$  cells in draining lymph nodes.

**Ex-Hobit<sup>+</sup> T cells accumulate in the circulation after reinfection.** To assess the contribution of  $T_{RM}$  cells to secondary T cell responses on pathogen reencounter, we generated Hobit lineage tracer mice by crossing Hobit reporter OT-I mice with *ROSA26-flox-stop-flox-eYFP* (*ROSA26-eYFP*) mice. The Hobit-controlled expression of Cre recombinase drives excision of an upstream transcriptional stop sequence in the *ROSA26-eYFP* reporter locus, resulting in constitutive expression of yellow fluorescent protein (YFP) in Hobit-expressing T cells (Extended Data Fig. 2a). The specificity and efficacy of YFP induction was monitored in memory T cells developing from tdTomato<sup>-</sup>YFP<sup>-</sup> naïve Hobit lineage tracer OT-I T cells after oral Lm-OVA infection. Primary  $T_{EM}$  and  $T_{CM}$  cells in the spleen, liver and MLNs did not substantially express tdTomato or YFP (Extended Data Fig. 2b,c). In contrast, the majority of  $T_{RM}$  cells in the liver and small intestine reported tdTomato expression and most tdTomato<sup>+</sup>  $T_{RM}$  cells expressed YFP. T cells coexpressing tdTomato and YFP exhibited higher Hobit expression than tdTomato<sup>+</sup>YFP<sup>-</sup> T cells, suggesting that Cre recombinase activity required a threshold of Hobit expression, which was not reached in all  $T_{RM}$  cells (Extended Data Fig. 2d). Both tdTomato<sup>+</sup>YFP<sup>-</sup> and tdTomato<sup>+</sup>YFP<sup>+</sup> populations were enriched for a  $T_{RM}$  phenotype (Extended Data Fig. 2e), indicating that tdTomato<sup>+</sup>YFP<sup>+</sup> cells were representative for the total Hobit<sup>+</sup>  $T_{RM}$  population. The highly selective expression of the YFP reporter in tdTomato<sup>+</sup>  $T_{RM}$  cells suggests that Hobit lineage tracer mice can be used to fate map  $T_{RM}$  cells during recall responses.

To assess the impact of antigen reencounter on Hobit expression in  $T_{RM}$  cells, intestinal tdTomato<sup>+</sup>YFP<sup>+</sup> OT-I  $T_{RM}$  cells were isolated and stimulated *in vitro* with MEC.B7.SigOVA cells expressing the cognate antigen OVA<sub>257–264</sub> and the costimulatory molecule CD80 (ref. 26). After antigenic stimulation, tdTomato<sup>+</sup>YFP<sup>+</sup>  $T_{RM}$  cells rapidly downregulated Hobit (tdTomato) expression (Fig. 3a,b), suggesting that antigen may trigger loss of the Hobit-driven phenotype of  $T_{RM}$  cells. To study the impact of antigen reencounter *in vivo*, we traced the offspring of Hobit<sup>+</sup>  $T_{RM}$  cells in rechallenge responses. Mice containing tdTomato<sup>-</sup>YFP<sup>-</sup> naïve Hobit lineage tracer OT-I T cells were sequentially infected with Lm-OVA via the oral route. After primary infection, very few circulating memory OT-I T cells expressed tdTomato or YFP (Fig. 3c). In contrast, a sizeable fraction of secondary effector and memory OT-I T cells expressed YFP, but not tdTomato, in the blood of rechallenged mice (Fig. 3c). Given the selective expression of YFP and tdTomato by  $T_{RM}$  cells before rechallenge, these ex-Hobit<sup>+</sup> (tdTomato<sup>-</sup>YFP<sup>+</sup>) cells were probably derived from  $T_{RM}$  cells that had downregulated Hobit expression in response to reinfection. The frequency of ex-Hobit<sup>+</sup> OT-I T cells in the blood increased sharply at day 8 post-infection and remained elevated until >30 d after reinfection, compared to the primary memory phase (Fig. 3d). A considerable increase in ex-Hobit<sup>+</sup> OT-I T cells was also observed in the spleen and liver, but not in lymph nodes or small intestine after reinfection (Fig. 3e–h), indicating that ex-Hobit<sup>+</sup> cells were restricted to the circulation. At the same time, reinfection resulted in increased numbers of  $T_{RM}$  cells (tdTomato<sup>+</sup>YFP<sup>+</sup>) in the liver and small intestine, but not in the spleen (Fig. 3f). A Hobit-expressing (YFP<sup>+</sup>tdTomato<sup>+</sup>)  $T_{RM}$  population was established in MLNs, but not in distant, peripheral lymph nodes, after oral reinfection (Fig. 3g,h). Reinfection consequently drove the expansion of pre-existing Hobit<sup>+</sup>  $T_{RM}$  populations in tissues and the accumulation of  $T_{RM}$  cells in draining lymph nodes. Taken together, we conclude that Hobit<sup>+</sup>  $T_{RM}$  cells generated considerable populations of secondary effector and memory T cells in the circulation, which downregulated Hobit expression in response to antigen recognition. Given the incomplete expression of YFP by

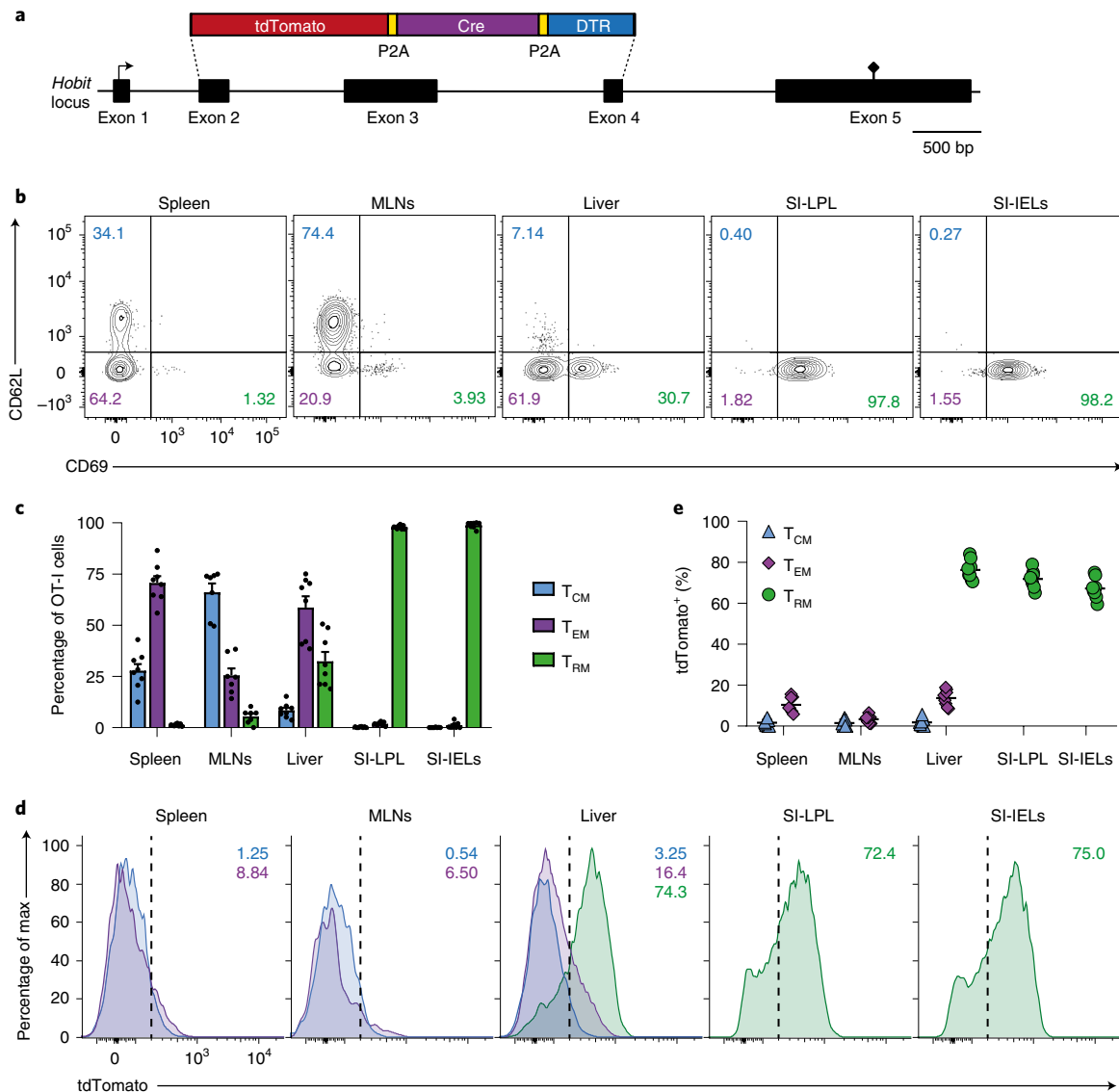


**Fig. 1 | Hobit identifies CD8<sup>+</sup> T<sub>RM</sub> cells across tissues after Lm-OVA infection.** **a**, Schematic representation depicting the *Hobit* locus of Hobit reporter mice and the targeting construct encoding the fluorescent protein tdTomato, Cre recombinase and DTR, separated by P2A sequences, which was integrated into the *Hobit* locus. **b–e**, Differentiation of congenically marked naive T cells of Hobit reporter OT-I mice into memory T cells was monitored in the spleen, MLNs, liver and SI-LPL lymphocytes and SI-IELs of recipient mice after oral infection with Lm-OVA. **b**, Representative flow cytometry plots showing the expression of CD69 and CD62L on Hobit reporter OT-I T cells to identify T<sub>CM</sub> (CD69<sup>+</sup>CD62L<sup>+</sup>), T<sub>EM</sub> (CD69<sup>+</sup>CD62L<sup>-</sup>) and T<sub>RM</sub> (CD69<sup>-</sup>CD62L<sup>-</sup>) cells. **c**, The frequencies of T<sub>CM</sub>, T<sub>EM</sub> and T<sub>RM</sub> cells in the indicated tissues were quantified. **d**, Representative histograms show tdTomato expression of Hobit reporter OT-I T cells with a T<sub>CM</sub>, T<sub>EM</sub> and T<sub>RM</sub> phenotype. **e**, Quantification of tdTomato expression is shown. Combined data from two independent experiments ( $n=8$  mice). The symbols represent individual mice; the bars represent the mean. The error bars represent the mean  $\pm$  s.e.m.

primary T<sub>RM</sub> cells, the contribution of Hobit<sup>+</sup> T<sub>RM</sub> cells to circulating secondary memory may be larger than observed using Hobit lineage tracer mice. Thus, Hobit<sup>+</sup> T<sub>RM</sub> cells contribute to systemic secondary effector and memory responses after reinfection.

**Hobit<sup>+</sup> T<sub>RM</sub> cells give rise to T<sub>EM</sub> cells on reinfection.** We next determined the phenotype of Hobit-expressing and ex-Hobit<sup>+</sup> memory T cells developing during secondary responses against Lm-OVA. The vast majority of YFP<sup>+</sup>tdTomato<sup>+</sup> OT-I T cells in the liver and MLNs expressed CD69 and lacked CD62L expression in line with a T<sub>RM</sub> phenotype (Fig. 4a–d). In contrast, ex-Hobit<sup>+</sup> OT-I T cells in the spleen and liver largely lacked CD69 expression (Fig. 4a,e), strongly indicating that these ex-Hobit<sup>+</sup> cells represent circulating memory T cells (consistent with their presence in the blood). Remarkably, ex-Hobit<sup>+</sup> memory T cells only contained a minor fraction of

CD62L<sup>+</sup> T<sub>CM</sub> cells compared to secondary memory T cells that never expressed Hobit (tdTomato<sup>-</sup>YFP<sup>-</sup>) (Fig. 4e,f), consistent with the absence of ex-Hobit<sup>+</sup> cells from the lymph nodes. Ex-Hobit<sup>+</sup> secondary memory T cells continued to express markedly lower levels of CD62L than their tdTomato<sup>-</sup>YFP<sup>-</sup> counterparts at later time points after rechallenge (>day 60), although the frequency of CD62L<sup>+</sup> T<sub>CM</sub> cells increased in both populations over time (Fig. 4g,h). Instead, ex-Hobit<sup>+</sup> secondary memory T cells largely consisted of T<sub>EM</sub> cells coexpressing KLRG1 and CX3CR1 (Fig. 4i,j). High expression of the surface receptors KLRG1 and CX3CR1 is associated with effector differentiation<sup>27–32</sup>. Taken together, the proportion of T<sub>RM</sub> cells that downregulate Hobit expression after rechallenge do not appear to persist as secondary T<sub>RM</sub> cells, exhibit limited ability to form T<sub>CM</sub> cells and mainly generate KLRG1<sup>+</sup>CX3CR1<sup>+</sup> T<sub>EM</sub> cells.

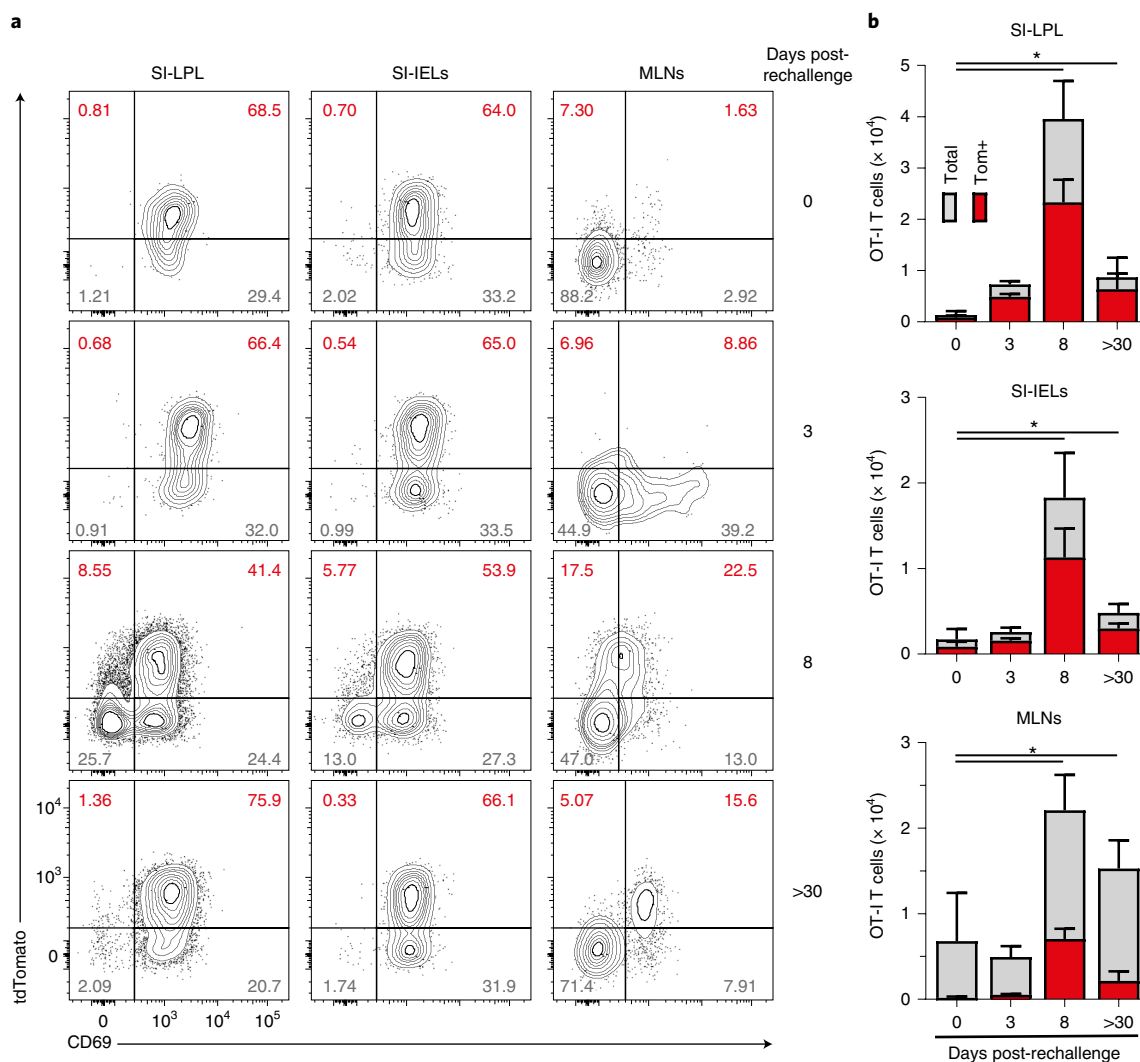


**Fig. 2 | Hobit<sup>+</sup> T<sub>RM</sub> cells expand locally and in draining lymph nodes after pathogen rechallenge.** Wild-type mice containing congenically marked naïve Hobit reporter OT-I T cells were orally infected and rechallenged with Lm-OVA. The response of the Hobit reporter OT-I T cells was analyzed in the memory phase after primary infection and in the effector or memory phase after secondary infection. **a**, Representative flow cytometry plots showing expression of CD69 and tdTomato by Hobit reporter OT-I T cells of SI-LPL (left) and SI-IELs (center) and MLNs (right) at the indicated time points post-Lm-OVA rechallenge. **b**, The number of total (gray) and tdTomato<sup>+</sup> (red) Hobit reporter OT-I T cells was quantified. A two-tailed Mann-Whitney *U*-test was used to compare the number of tdTomato<sup>+</sup> OT-I T cells at different time points, \**P* < 0.05. Data are representative of two independent experiments (*n* = 4 or 5 mice). The bars represent the mean; the error bars represent the mean ± s.e.m.

**Ex-T<sub>RM</sub> cells are transcriptionally and functionally distinct.** To further characterize ex-Hobit<sup>+</sup> secondary memory T cells arising after reinfection, we performed transcriptional profiling by RNA sequencing (RNA-seq) of naïve, primary and secondary memory T cells that developed in response to Lm-OVA infection. Principal component analysis revealed that primary T<sub>RM</sub> cells from the liver and small intestine formed discrete populations, which separated from each other as well as from circulating naïve and memory T cell populations at the transcriptional level (Fig. 5a). Primary and secondary T<sub>CM</sub> cells formed distinct, but closely related populations, similar to primary and secondary T<sub>EM</sub> cells. Ex-Hobit<sup>+</sup> secondary T<sub>EM</sub> cells separated from both T<sub>CM</sub> and T<sub>RM</sub> subsets and clustered more closely with other T<sub>EM</sub> populations (Fig. 5a,b). Compared to primary liver T<sub>RM</sub> cells, ex-Hobit<sup>+</sup> secondary T<sub>EM</sub> cells had downregulated expression of T<sub>RM</sub> signature genes, including *Xcl1*, *Rgs1*, *Osgin1* and *P2rx7* (refs. <sup>8,9,33</sup>), and upregulated pathways involved in lymphocyte migration, for example, *S1pr1*, *S1pr5* and *Klf2* (Fig. 5c) (refs. <sup>34,35</sup>). Importantly, transcriptional differences were also

observed between secondary ex-Hobit<sup>+</sup> T<sub>EM</sub> cells and both primary and secondary YFP<sup>-</sup> T<sub>EM</sub> cells that had never expressed Hobit (Fig. 5b,d). Interestingly, genes with reduced expression in secondary ex-Hobit<sup>+</sup> T<sub>EM</sub> cells compared to secondary YFP<sup>-</sup> T<sub>EM</sub> cells included *Dapl1* and *Eomes* (Fig. 5d), which have been previously reported to be specifically downregulated in memory CD8<sup>+</sup> T cells after repeated antigen stimulation<sup>36</sup>.

To investigate the protective impact of the secondary T<sub>EM</sub> populations, we transferred equal numbers of ex-Hobit<sup>+</sup> and YFP<sup>-</sup> secondary T<sub>EM</sub> cells into naïve recipient mice before Lm-OVA infection (Fig. 5e). Neither donor population substantially influenced the bacterial burden in the spleen on day 3 post-infection (Fig. 5f). In contrast, mice that received ex-Hobit<sup>+</sup> secondary T<sub>EM</sub> cells tended to have lower bacterial loads in the small intestine and exhibited considerably reduced bacterial loads in MLNs, compared to mice that received secondary YFP<sup>-</sup> T<sub>EM</sub> cells or mice that did not receive donor cells. Hence, ex-Hobit<sup>+</sup> secondary T<sub>EM</sub> cells appeared to have higher protective potential than their counterparts without prior

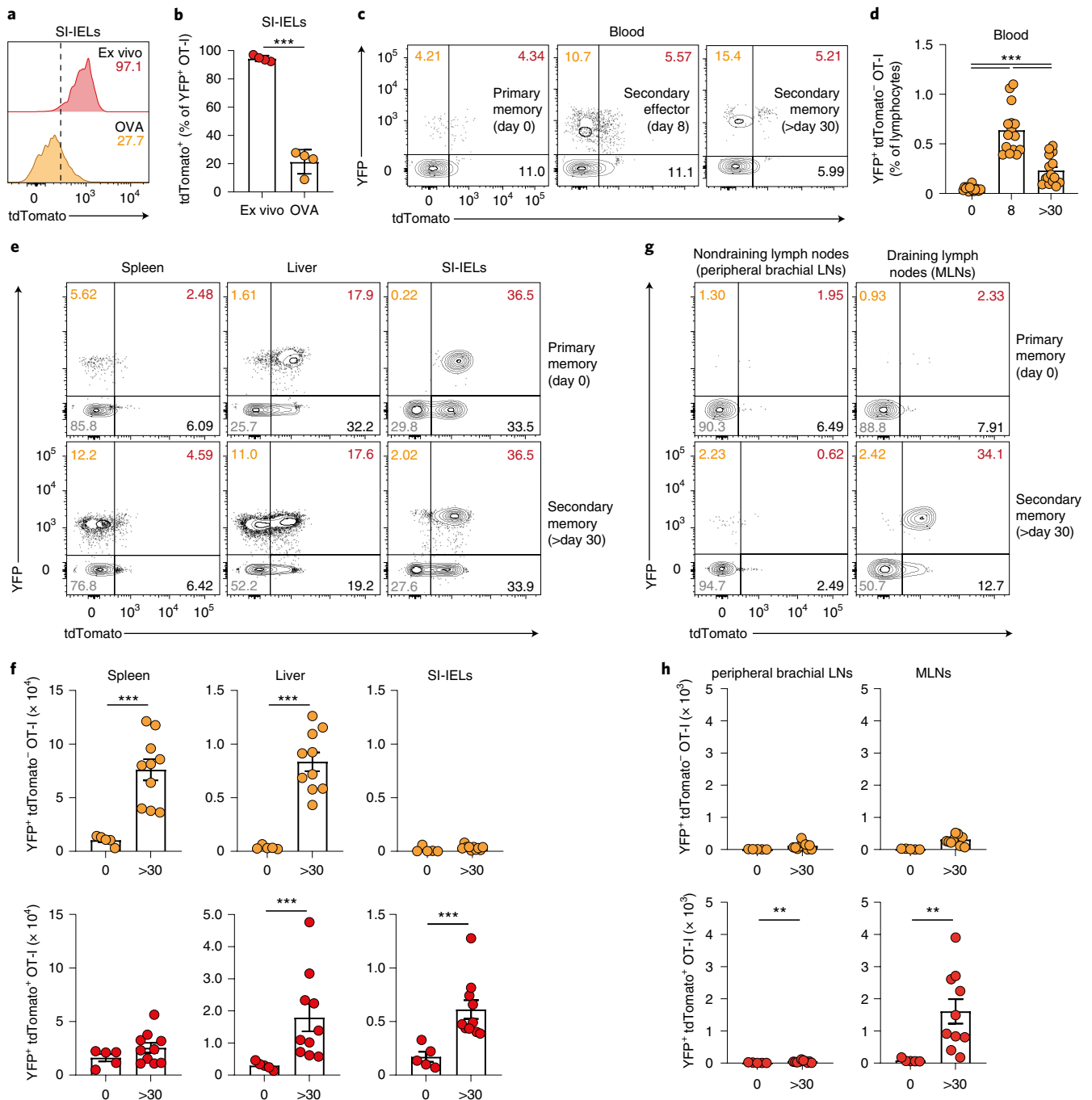


**Fig. 3 | Hobit<sup>+</sup> T<sub>RM</sub> cells downregulate Hobit expression on antigen encounter and form circulating memory cells after pathogen rechallenge.**

**a, b**, Hobit (tdTomato) expression by primary Hobit reporter × ROSA26-eYFP OT-I T<sub>RM</sub> cells from the SI-IELs arising after oral Lm-OVA infection was assessed ex vivo and 3 d after in vitro stimulation with MEC.B7.SigOVA cells. **a**, Representative histograms showing tdTomato expression by YFP<sup>+</sup> Hobit reporter × ROSA26-eYFP OT-I T cells. **b**, The frequency of tdTomato<sup>+</sup> cells within the YFP<sup>+</sup> population was quantified (two-tailed paired *t*-test, \*\*\**P* = 0.0003). **c–h**, The phenotype and number of adoptively transferred Hobit reporter × ROSA26-eYFP OT-I T cells was analyzed after primary and secondary oral infection with Lm-OVA. **c**, Representative flow cytometry plots showing the expression of YFP and tdTomato by Hobit reporter × ROSA26-eYFP OT-I T cells in blood. **d**, The frequency of ex-Hobit<sup>+</sup> (YFP<sup>+</sup>tdTomato<sup>-</sup>) OT-I T cells within the lymphocyte population was quantified in blood (two-tailed paired *t*-test, \*\*\**P* < 0.0001). **e**, The expression of YFP and tdTomato is displayed for Hobit reporter × ROSA26-eYFP OT-I T cells in the spleen, liver and SI-IELs >30 d after primary infection (top row) and >30 d after secondary infection (bottom row). **f**, Ex-Hobit<sup>+</sup> (YFP<sup>+</sup>tdTomato<sup>-</sup>) and Hobit<sup>+</sup> (YFP<sup>+</sup>tdTomato<sup>+</sup>) Hobit reporter × ROSA26-eYFP OT-I T cells were enumerated in the spleen, liver and SI-IELs before (0) and in memory phase after Lm-OVA rechallenge (>30). Two-tailed Mann-Whitney *U*-test, \*\*\**P* < 0.001. **g**, Representative flow cytometry plots showing the expression of YFP and tdTomato by Hobit reporter × ROSA26-eYFP OT-I T cells in nondraining (peripheral brachial lymph nodes) and draining (MLNs) lymph nodes. **h**, Ex-Hobit<sup>+</sup> (YFP<sup>+</sup>tdTomato<sup>-</sup>) and Hobit<sup>+</sup> (YFP<sup>+</sup>tdTomato<sup>+</sup>) Hobit reporter × ROSA26-eYFP OT-I T cells were enumerated in peripheral brachial lymph nodes and MLNs before (0) and in memory phase after Lm-OVA rechallenge (>30). Two-tailed Mann-Whitney *U*-test, \*\*\**P* < 0.008 (peripheral brachial lymph nodes), \*\**P* < 0.0013 (MLNs). **a, b**, Representative data from two independent experiments (*n* = 4 mice). **c–h**, Combined data from two independent experiments (*n* = 5, 10 or 15 mice). Symbols represent individual mice; bars represent the mean. Error bars represent mean ± s.e.m.

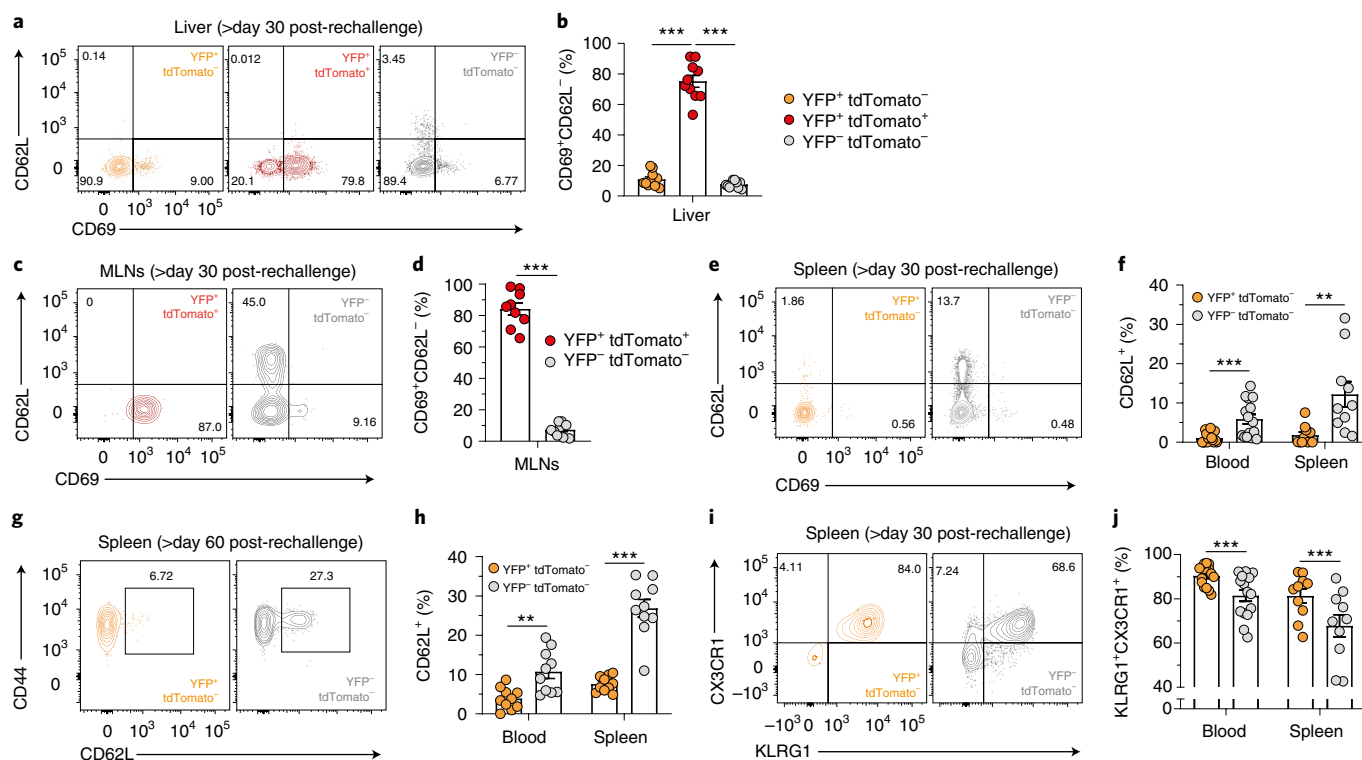


**Fig. 4 | Ex-Hobit<sup>+</sup> T cells primarily acquire a T<sub>EM</sub> phenotype after pathogen rechallenge.** The phenotype of adoptively transferred Hobit reporter × ROSA26-eYFP OT-I T cells was analyzed after secondary oral infection with Lm-OVA. **a–h**, Expression of CD62L and CD69 on the indicated fractions of secondary memory Hobit reporter × ROSA26-eYFP OT-I T cells, as defined by YFP and tdTomato expression in the liver, MLNs and spleen, was analyzed at the indicated time points. **a, c, e, g**, Representative flow cytometry plots are shown and the frequency of T<sub>RM</sub> (CD69<sup>+</sup>CD62L<sup>-</sup>) (**b, d**) and T<sub>CM</sub> cells (CD62L<sup>+</sup>) (**f, h**) was quantified within the indicated populations of Hobit reporter × ROSA26-eYFP OT-I T cells. Two-tailed paired *t*-test, \*\**P* < 0.01, \*\*\**P* < 0.001. **i**, Representative flow cytometry plots showing expression of CX3CR1 and KLRG1 on the indicated fractions of secondary memory Hobit reporter × ROSA26-eYFP OT-I T cells in the spleen. **j**, The frequencies of KLRG1 and CX3CR1 coexpression were analyzed in ex-Hobit<sup>+</sup> (YFP<sup>+</sup>tdTomato<sup>-</sup>) and control (YFP<sup>-</sup>tdTomato<sup>-</sup>) Hobit reporter × ROSA26-eYFP OT-I T cells in the blood and spleen. Two-tailed paired *t*-test, \*\*\**P* < 0.001. Combined data from two independent experiments with *n* = 9 mice (**d**) or *n* = 10 or 15 mice (**b, f, h, j**). The symbols represent individual mice; the bars represent the mean. The error bars represent the mean ± s.e.m.

Hobit expression, in particular in lymph nodes draining mucosal tissues. Taken together, circulating secondary memory cells arising from T<sub>RM</sub> cells form a distinct T<sub>EM</sub> population with enhanced capacity to protect against reinfection.

#### Intestinal and liver T<sub>RM</sub> cells form systemic recall responses.

During recall responses, T<sub>CM</sub> cells undergo extensive proliferation and give rise to secondary circulating memory T cells<sup>3,23</sup>. Given that T<sub>RM</sub> cells appear to contribute to systemic secondary responses on reinfection, we asked how these responses compare to T<sub>CM</sub> recall responses. Previously, liver-resident T<sub>RM</sub> cells were successfully reintroduced to the liver after intravenous injection into donor mice<sup>37</sup>, indicating that the rechallenge potential of donor T<sub>RM</sub> cells can be studied using an adoptive transfer strategy. To this end, we isolated intestinal T<sub>RM</sub> cells and, for comparison, splenic T<sub>CM</sub> cells from lymphocytic choriomeningitis virus (LCMV)-immune mice at >30 d after LCMV (Armstrong) infection. The purity of the subsets before transfer was >98% for T<sub>CM</sub> cells and >99% for T<sub>RM</sub> cells (Extended Data Fig. 3a). Congenically marked T<sub>CM</sub> and T<sub>RM</sub> cells containing equal amounts of T<sub>CM</sub> and T<sub>RM</sub> cells specific for the immunodominant gp33 epitope of LCMV (D<sup>b</sup>GP33<sup>+</sup>) were cotransferred into naïve mice and recipients were analyzed two weeks after transfer (Extended Data Fig. 3a,b). Donor T<sub>CM</sub> cells were present in the blood, spleen, MLNs and liver of recipient mice, while donor T<sub>RM</sub> cells were only detected in the liver (Extended Data Fig. 3c,d). Both subsets were absent from the small intestine after transfer.

The respective phenotypes of T<sub>CM</sub> and T<sub>RM</sub> cells were largely preserved after transfer (Extended Data Fig. 3e,f). Importantly, LCMV-specific T cells were detectable in both donor populations (Extended Data Fig. 3g). Similar observations were made after adoptive cotransfer of monoclonal Hobit reporter OT-I T<sub>RM</sub> and T<sub>CM</sub> cells isolated from the SI-IELs and spleen of Lm-OVA-infected mice, respectively (Extended Data Fig. 4). Notably, donor T<sub>RM</sub> cells maintained high expression of Hobit in the liver following transfer (Extended Data Fig. 4g,h). Thus, donor populations of pathogen-specific T<sub>RM</sub> cells were successfully established on adoptive transfer, suggesting opportunity to examine the secondary responses of donor T<sub>RM</sub> cells.

After LCMV challenge, donor T<sub>CM</sub> and T<sub>RM</sub> cells formed responses of virus-specific effector and memory T cells in the blood, spleen and liver of recipient mice (Fig. 6a). Effector T cells of T<sub>CM</sub> and T<sub>RM</sub> origin nearly uniformly expressed the proliferation-associated molecule Ki-67, indicating substantial proliferation on pathogen reencounter (Fig. 6b,c). T<sub>CM</sub>-derived effector and memory T cells were present at higher frequencies throughout tissues, suggesting that T<sub>CM</sub> cells expanded more vigorously compared to T<sub>RM</sub> cells after rechallenge (Fig. 6a,b). Thus, intestinal T<sub>RM</sub> cells contributed systemically to effector and memory responses after reinfection, albeit with a lower output on a per-cell basis compared to T<sub>CM</sub> cells. Next, we analyzed the phenotype of the secondary memory T cells developing from T<sub>CM</sub> and T<sub>RM</sub> cells. Donor T<sub>CM</sub> cells re-formed secondary CD62L<sup>+</sup> T<sub>CM</sub> cells in the spleen and MLNs, while T<sub>RM</sub>-derived

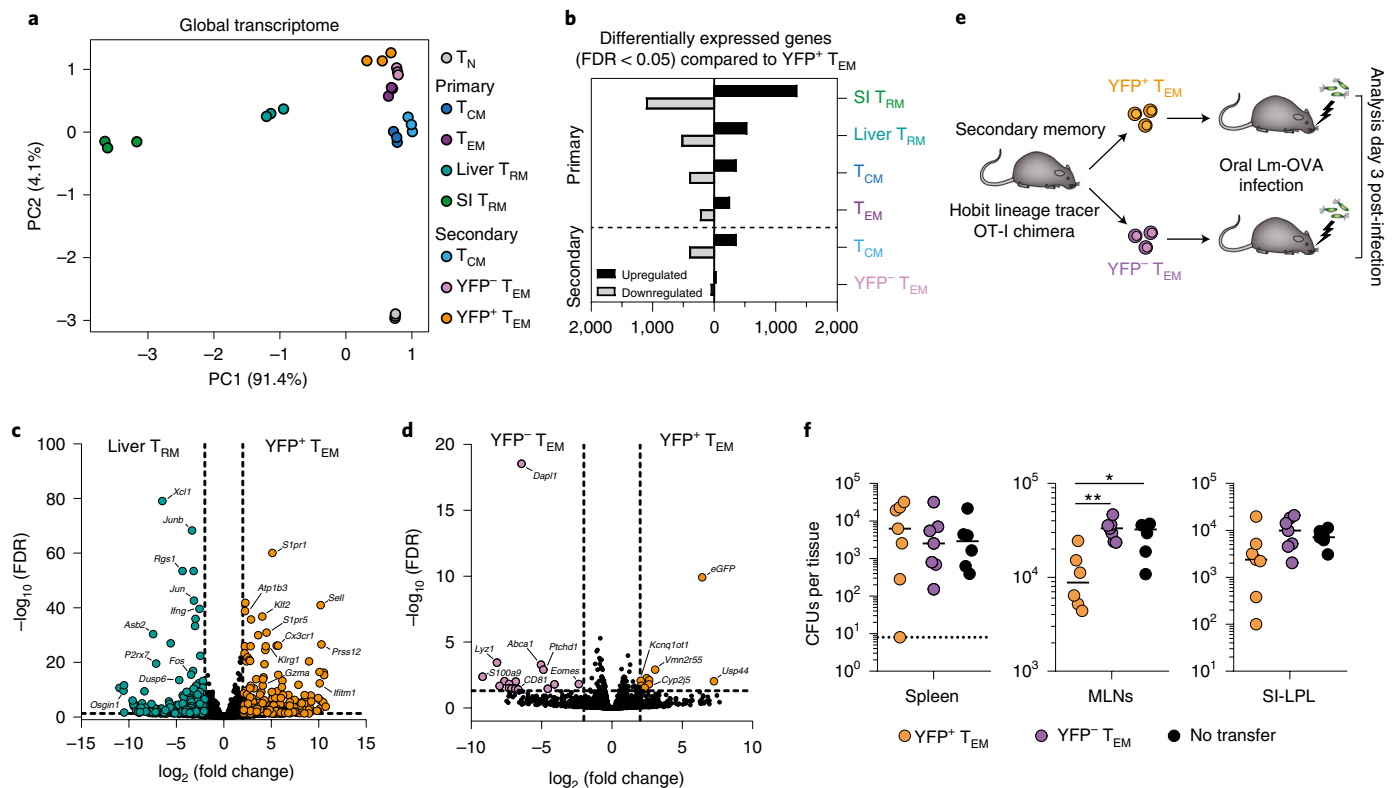


**Fig. 5 | Secondary ex-Hobit<sup>+</sup> T cells constitute a transcriptionally and functionally distinct effector memory subset.** Primary and secondary memory Hobit reporter × ROSA26-eYFP OT-I T cell subsets were isolated for transcriptional and functional analysis after oral infection with Lm-OVA. **a**, Principal component analysis of RNA-seq data for naïve (T<sub>N</sub>), primary memory and secondary memory OT-I T cells. **b**, Number of differentially upregulated (black) or downregulated genes (gray) in secondary YFP<sup>+</sup> T<sub>EM</sub> cells compared with the indicated subsets (FDR < 0.05). **c,d**, Volcano plots show differentially expressed genes (FDR < 0.05, log<sub>2</sub>(fold change) > 2) between secondary YFP<sup>+</sup> T<sub>EM</sub> cells and primary liver T<sub>RM</sub> cells (**c**), and secondary YFP<sup>+</sup> and YFP<sup>-</sup> T<sub>EM</sub> cells (**d**) as determined by RNA-seq. **e**, Graphic depicting the setting used to determine the protective capacity of secondary memory OT-I T cells. Briefly, secondary memory YFP<sup>+</sup> and YFP<sup>-</sup> T<sub>EM</sub> cells were FACS-purified from the spleen of Lm-OVA-infected mice and transferred into naïve recipients, which were subsequently challenged with Lm-OVA. The bacterial loads in tissues were determined at 3 d post-infection. **f**, The CFUs of Lm-OVA were determined in the indicated tissues of recipient and control mice (no cell transfer) at 3 d post-infection. Two-tailed Mann-Whitney *U*-test, \**P* = 0.026, \*\**P* = 0.0047. **a–d**, Data from one experiment (*n* = 3 pooled samples). **f**, Combined data from two independent experiments (*n* = 6 or 7 mice). The symbols represent pooled samples from 3–4 mice (**a**), individual mice (**f**) or genes (**c,d**); the bars represent the number of differentially expressed genes (**b**) or the median (**f**). **b–d**, Quasi-likelihood *F*-test as implemented in edgeR glmFit with Benjamini-Hochberg correction for multiple testing.

secondary memory T cells were largely unable to generate T<sub>CM</sub> cells (Fig. 6d,e) and were absent from lymph nodes (Fig. 6a). Instead, T<sub>RM</sub>-derived secondary memory T cells in the spleen almost exclusively coexpressed KLRG1 and CX3CR1 and displayed a T<sub>EM</sub> phenotype (Fig. 6f,g). Both T<sub>CM</sub> and T<sub>RM</sub> cells formed secondary CD69<sup>+</sup> T<sub>RM</sub> cells in the liver and small intestine (Fig. 6h–k). T<sub>RM</sub> cells outperformed T<sub>CM</sub> cells in establishing secondary T<sub>RM</sub> cells in these tissues, particularly in the small intestine, their tissue of origin (Fig. 6h–k). We made similar observations using adoptively cotransferred monoclonal populations of Hobit reporter OT-I T<sub>RM</sub> and T<sub>CM</sub> cells (Extended Data Fig. 5). Importantly, donor OT-I T<sub>RM</sub> cells formed secondary KLRG1<sup>+</sup>CX3CR1<sup>+</sup> T<sub>EM</sub> cells after Lm-OVA challenge (Extended Data Fig. 5). Taken together, T<sub>CM</sub> cells retained the ability to regenerate the entire spectrum of memory T cell subsets. In contrast, T<sub>RM</sub> cells were compromised in forming secondary T<sub>CM</sub> cells and preferentially developed into secondary T<sub>EM</sub> and T<sub>RM</sub> cells, in line with our findings from the T<sub>RM</sub> fate mapping experiments.

Given that donor intestinal T<sub>RM</sub> cells appear to settle predominantly in the liver after intravenous injection, we next examined the ability of liver T<sub>RM</sub> cells to form recall responses. To address this point, we cotransferred intestinal and liver T<sub>RM</sub> cells into naïve recipient mice and challenged these mice with LCMV two weeks after transfer (Extended Data Fig. 6a). Both T<sub>RM</sub> populations gave rise

to virus-specific effector and memory responses at similar frequencies in the blood, spleen and liver after LCMV challenge (Extended Data Fig. 6b). Similar to intestinal T<sub>RM</sub> cells, liver T<sub>RM</sub> cells poorly developed into secondary CD62L<sup>+</sup> T<sub>CM</sub> cells but efficiently formed secondary KLRG1<sup>+</sup>CX3CR1<sup>+</sup> T<sub>EM</sub> cells in the spleen (Extended Data Fig. 6c–f). As observed earlier, intestinal T<sub>RM</sub> cells formed secondary T<sub>RM</sub> cells in the liver after reactivation; cells of liver T<sub>RM</sub> origin did this at similar frequencies (Extended Data Fig. 6g,h). Thus, T<sub>RM</sub> cells from different tissues, namely liver and intestine, form secondary effector and memory responses in the circulation and give rise to secondary T<sub>RM</sub> and T<sub>EM</sub> cells after reinfection.

**T<sub>RM</sub> cells substantially contribute to secondary T<sub>RM</sub> and T<sub>EM</sub> formation.** T<sub>RM</sub> cells are abundantly present in peripheral tissues after acute infections; recent evidence suggests that immunosurveillance of nonlymphoid tissues is primarily executed by local resident populations<sup>10</sup>. Given their capacity to form secondary T<sub>RM</sub> and T<sub>EM</sub> cells after pathogen rechallenge, we next set out to investigate the total contribution of T<sub>RM</sub> cells to secondary responses. To visualize the impact of T<sub>RM</sub> cells on recall responses after reinfection, we developed a competitive setting, which allows for specific ablation of T<sub>RM</sub> cells while leaving the circulating populations intact. To this end, naïve mice received cotransfers of wild-type and Hobit

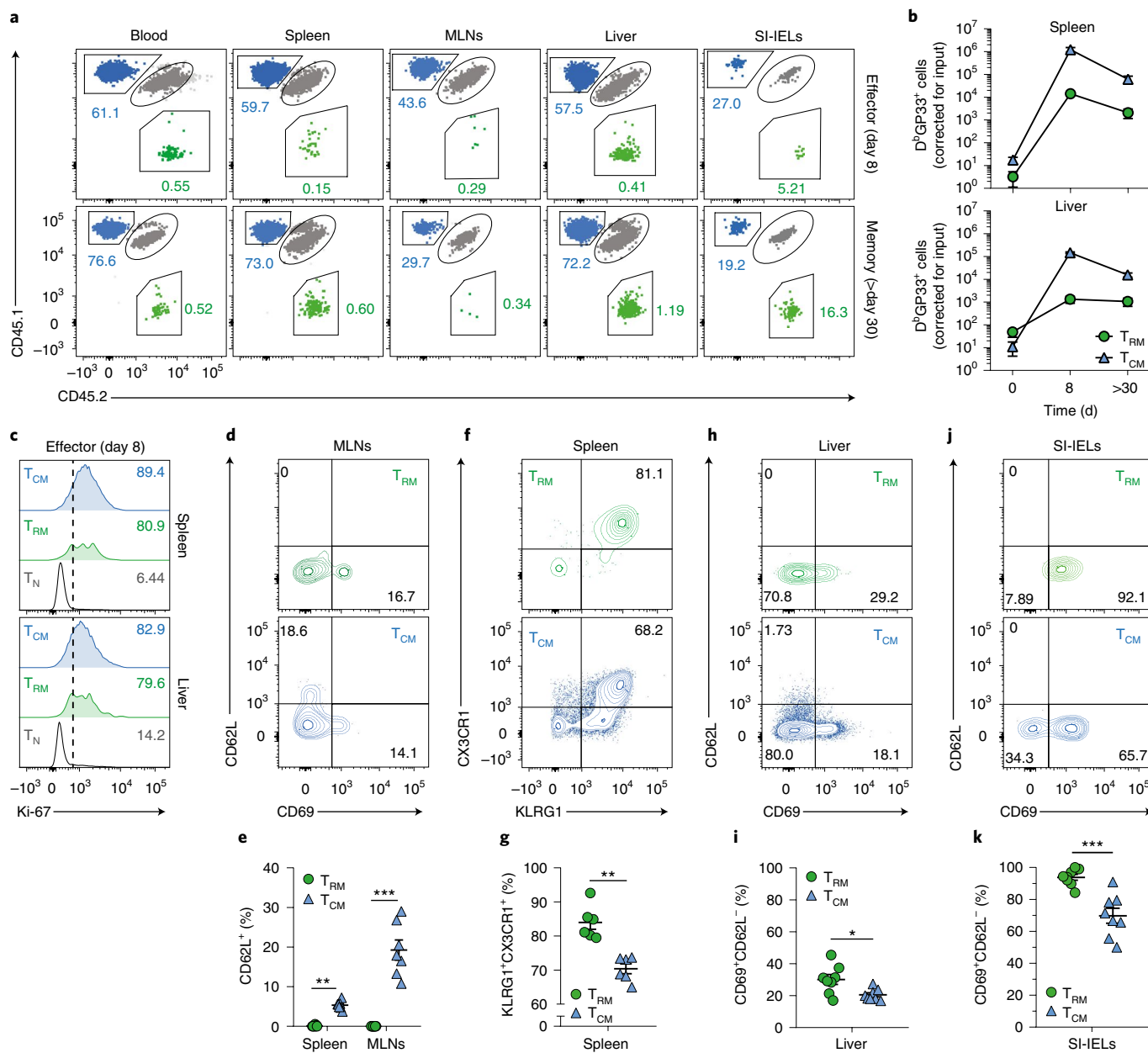


**Fig. 6 | CD8<sup>+</sup> T<sub>RM</sub> cells generate systemic responses on pathogen rechallenge.** Congenically marked T<sub>RM</sub> and T<sub>CM</sub> cells were FACS-purified from the SI-IELs and spleen of LCMV-infected mice, respectively, and cotransferred into naïve recipients, which were challenged with LCMV 14 d later. The offspring of the virus-specific (D<sup>b</sup>GP33<sup>+</sup>) donor T cells were analyzed at 8 and >30 d post-infection. **a**, Representative flow cytometry plots showing expression of the congenic markers CD45.1 and CD45.2 used to identify donor T<sub>RM</sub>-derived (green), donor T<sub>CM</sub>-derived (blue) and host-derived (gray) cells in the D<sup>b</sup>GP33<sup>+</sup> T cell population in the indicated tissues at 8 and >30 d post-infection. **b**, The number of T<sub>RM</sub>- and T<sub>CM</sub>-derived D<sup>b</sup>GP33<sup>+</sup> cells (corrected for input ratio at the time of transfer) was determined in the spleen and liver at the indicated time points before and after LCMV challenge. **c**, Representative histograms showing the expression of Ki-67 by D<sup>b</sup>GP33<sup>+</sup> T<sub>RM</sub>- and T<sub>CM</sub>-derived effector T cells, and CD44<sup>low</sup>CD62L<sup>+</sup> naïve CD8<sup>+</sup> T (T<sub>N</sub>) cells in the spleen and liver at 8 d post-infection. **d,f**, Representative flow cytometry plots showing the expression of CD62L and CD69 on D<sup>b</sup>GP33<sup>+</sup> T<sub>RM</sub>- and T<sub>CM</sub>-derived memory T cells in the spleen (**d**) and expression of CX3CR1 and KLRG1 on D<sup>b</sup>GP33<sup>+</sup> T<sub>RM</sub>- and T<sub>CM</sub>-derived memory T cells in the spleen (**f**) at >30 d after LCMV challenge. **e,g**, The frequency of CD62L expression (**e**) and KLRG1 and CX3CR1 coexpression (**g**) in the offspring of donor T<sub>RM</sub> and T<sub>CM</sub> populations was quantified. Two-tailed paired *t*-test, \*\**P* < 0.01, \*\*\**P* < 0.001. **h,j**, Representative flow cytometry plots showing the expression of CD62L and CD69 of D<sup>b</sup>GP33<sup>+</sup> secondary memory cells developing from donor T<sub>RM</sub> or T<sub>CM</sub> cells in the liver (**h**) and SI-IELs (**j**) after LCMV challenge. **i,k**, Frequency of T<sub>RM</sub> cells (CD69<sup>+</sup>CD62L<sup>-</sup>) within the donor populations in the liver (**i**) and SI-IELs (**k**) were quantified. Two-tailed paired *t*-test, \**P* = 0.0155, \*\*\**P* = 0.0006. Combined data from three independent experiments (*n* = 6 or 8 mice). **b**, The symbols represent the mean or individual mice (**e,g,i,k**). The bars represent the mean. The error bars represent the mean ± s.e.m.

reporter OT-I T cells before Lm-OVA infection. In the memory phase after infection, mice were treated with diphtheria toxin (DT) to specifically deplete Hobit<sup>+</sup> OT-I T cells of the Hobit reporter compartment. Administration of DT resulted in a strong reduction

of Hobit<sup>+</sup> OT-I T cells in the liver and small intestine compared to control mice (Extended Data Fig. 7a,b). In line with the selective expression pattern of Hobit in the memory subsets, depletion of Hobit<sup>+</sup> cells translated into a substantially reduced contribution of

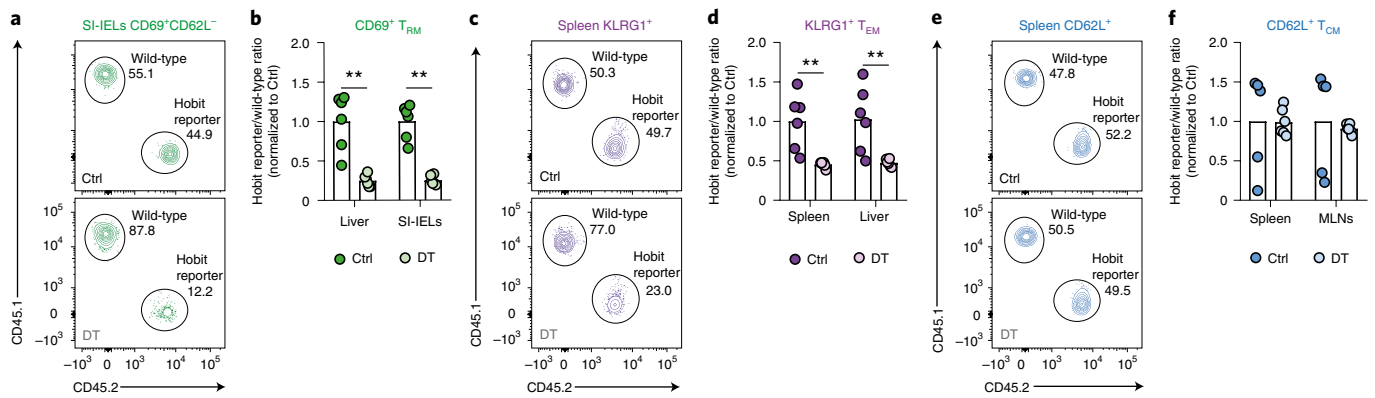


**Fig. 7 | Formation of secondary CD8<sup>+</sup> T<sub>RM</sub> and T<sub>EM</sub> cells depends on primary Hobit<sup>+</sup> T cells.** Wild-type mice containing congenically marked naïve wild-type and Hobit reporter OT-I T cells were infected orally with Lm-OVA. DT was administered in the memory phase after infection to specifically deplete Hobit reporter T<sub>RM</sub> cells. After depletion, mice were rechallenged orally with Lm-OVA and the secondary memory of wild-type and Hobit reporter OT-I T cells was analyzed. **a–f**, The contribution of wild-type and Hobit reporter OT-I T cells to the formation of secondary memory populations was analyzed in control and DT-treated mice at >30 d post-Lm-OVA rechallenge. **a, c, e**, Representative flow cytometry plots showing the expression of the congenic markers CD45.1 and CD45.2 used to identify the contribution of wild-type (CD45.1<sup>+</sup>) and Hobit reporter (CD45.2<sup>+</sup>) OT-I T cells to the formation of CD69<sup>+</sup> T<sub>RM</sub> cells in the SI-IELs (**a**), KLRG1<sup>+</sup> T<sub>EM</sub> cells in the spleen (**c**) and CD62L<sup>+</sup> T<sub>CM</sub> cells in the spleen (**e**) under control conditions (top) and after DT treatment (bottom). **b, d, f**, The ratio between Hobit reporter and wild-type OT-I T cells was determined under control conditions and after DT treatment for the CD69<sup>+</sup> T<sub>RM</sub> population of the liver and SI-IELs (**b**), the KLRG1<sup>+</sup> T<sub>EM</sub> population of the spleen and liver (**d**) and the CD62L<sup>+</sup> T<sub>CM</sub> population of the spleen and MLNs (**f**). Ratios were normalized to controls. Two-tailed Mann-Whitney *U*-test, \*\**P* < 0.01. Data from one experiment (*n* = 6 mice). The symbols represent individual mice; the bars represent the mean.

Hobit reporter cells in the T<sub>RM</sub> compartment, while their contribution to the T<sub>CM</sub> compartment remained unaffected (Extended Data Fig. 7c–h). Of note, DT administration also reduced the presence of Hobit reporter OT-I T cells within the T<sub>EM</sub> compartment (Extended Data Fig. 7f,i), which may have resulted from the limited Hobit expression by T<sub>EM</sub> cells. After Lm-OVA rechallenge, the formation of secondary T<sub>RM</sub> cells in both liver and small intestine was strongly compromised in the Hobit reporter but not in the wild-type compartment of DT-treated mice compared to control mice (Fig. 7a,b). DT treatment also impaired the generation of secondary KLRG1<sup>+</sup> T<sub>EM</sub> cells by the Hobit reporter compartment relative to the T<sub>RM</sub>-sufficient wild-type compartment after rechallenge (Fig. 7c,d). No impact was observed on the formation of secondary CD62L<sup>+</sup> T<sub>CM</sub> cells by Hobit reporter OT-I T cells after DT treatment (Fig. 7e,f). Taken together, these data suggest that primary T<sub>RM</sub> cells substantially contribute to secondary T<sub>RM</sub> cell formation and may contribute to the generation of secondary T<sub>EM</sub> cells.

Given the impact of DT treatment on the primary T<sub>EM</sub> compartment (Extended Data Fig. 7), it is not possible to fully exclude a contribution of primary T<sub>EM</sub> cells to secondary responses using the Hobit-driven DTR system. Therefore, we developed a complementary approach to investigate the contribution of T<sub>RM</sub> cells to secondary responses more stringently. To this end, naïve mice received cotransfers of wild-type OT-I T cells and OT-I T cells with a genetic deletion of the purinergic receptor P2RX7 (*P2rx7*<sup>-/-</sup> OT-I). In agreement with earlier findings<sup>33</sup>, P2RX7 deficiency did not impair the formation of T<sub>RM</sub>, T<sub>CM</sub> and T<sub>EM</sub> cells from adoptively transferred naïve OT-I T cells after oral Lm-OVA infection (Extended Data Fig. 8a–d). We have previously demonstrated that P2RX7 is specifically expressed by T<sub>RM</sub> cells but not by circulating memory T cells, and that P2RX7 activation *in vivo* by extracellular nucleotides, such as NAD<sup>+</sup>, results in depletion of T<sub>RM</sub> cells while retaining T<sub>CM</sub> and T<sub>EM</sub> cells<sup>33</sup>. Treatment with exogenous NAD<sup>+</sup> resulted in the selective ablation of the wild-type compartment of T<sub>RM</sub> cells, while the *P2rx7*<sup>-/-</sup> compartment of T<sub>RM</sub> cells and circulating memory T cells of both compartments remained unaffected (Extended Data Fig. 8a–d). The impact of NAD<sup>+</sup> on other P2RX7-expressing lymphocytes, including host CD4<sup>+</sup> T<sub>H1</sub> cells and TCRγδ T cells, was

already reversed through repopulation at two weeks after NAD<sup>+</sup> treatment (Extended Data Fig. 8e–g). Therefore, mice were rechallenged with Lm-OVA two weeks after NAD<sup>+</sup> treatment to analyze the contribution of the wild-type and *P2rx7*<sup>-/-</sup> OT-I compartments to the secondary memory response.

The formation of secondary T<sub>RM</sub> cells in both liver and small intestine was strongly compromised in the wild-type, but not the *P2rx7*<sup>-/-</sup> compartment, after NAD<sup>+</sup>-driven depletion of wild-type T<sub>RM</sub> cells before rechallenge (Fig. 8a,b). Interestingly, the development of secondary T<sub>RM</sub> cells in the intestine-draining MLNs was also strongly impaired in the wild-type but not the *P2rx7*<sup>-/-</sup> compartment (Fig. 8c,d). These data suggest that secondary T<sub>RM</sub> cells in peripheral tissues and draining lymph nodes primarily develop from pre-existing T<sub>RM</sub> populations. NAD<sup>+</sup>-mediated depletion of wild-type T<sub>RM</sub> cells impaired the generation of secondary KLRG1<sup>+</sup> T<sub>EM</sub> cells by the wild-type compartment relative to the T<sub>RM</sub>-sufficient *P2rx7*<sup>-/-</sup> compartment after rechallenge (Fig. 8e,f). In contrast, T<sub>RM</sub> ablation had no impact on the formation of secondary CD62L<sup>+</sup> T<sub>CM</sub> cells by wild-type OT-I T cells after Lm-OVA reinfection (Fig. 8g,h). Therefore, we conclude that primary T<sub>RM</sub> cells substantially contribute to the formation of not only secondary T<sub>RM</sub> cells, but also circulating T<sub>EM</sub> cells after reinfection. These findings indicate that a large fraction of circulating secondary memory T cells originates from T<sub>RM</sub> populations.

## Discussion

Mucosal tissues are frequently exposed to pathogens and T<sub>RM</sub> cells are critical in providing protection against these invaders<sup>11,12</sup>. Based on the T<sub>RM</sub>-restricted expression of the transcription factor Hobit<sup>9,38</sup>, we developed the Hobit reporter mouse as a new tool to identify T<sub>RM</sub> cells and trace their progeny during recall responses. Using these mice and complementary adoptive transfer and selective depletion experiments, we found that reinfection drove T<sub>RM</sub> cell expansion in peripheral tissues and draining lymph nodes, and the development of a secondary T<sub>EM</sub> population downstream of T<sub>RM</sub> cells.

On reactivation, T<sub>RM</sub> cells in the skin and female reproductive tract rapidly exert effector functions, undergo local proliferation and contribute to maintenance of the local memory pool<sup>13,14,39–41</sup>.

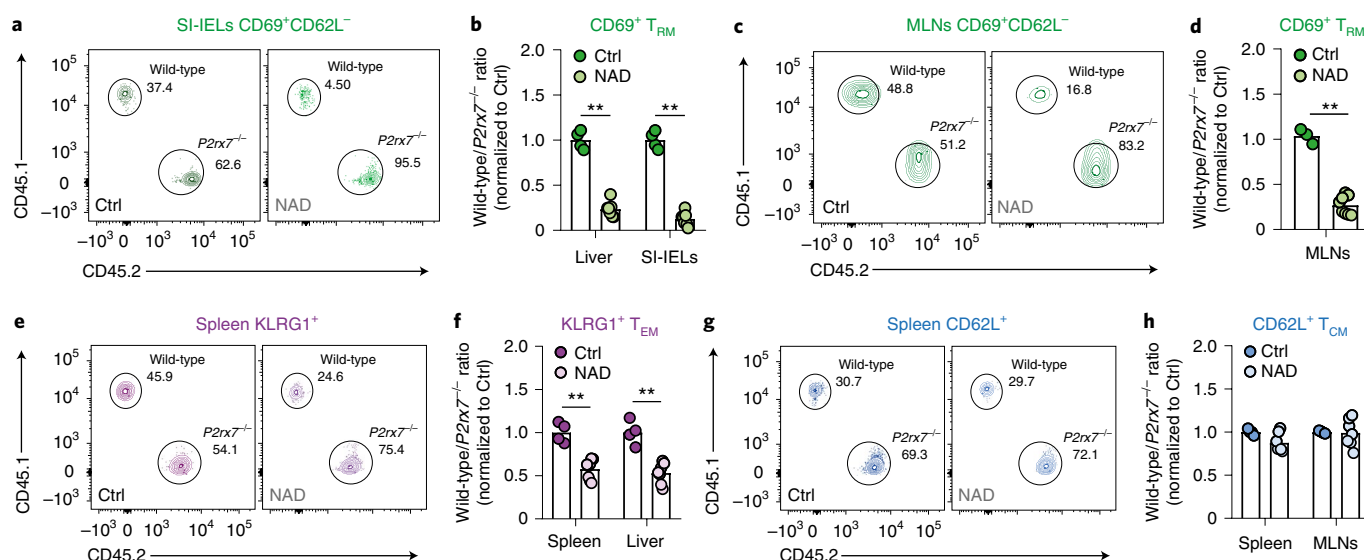


**Fig. 8 | CD8<sup>+</sup> T<sub>RM</sub> cells substantially contribute to secondary memory responses after pathogen rechallenge.** Wild-type mice containing congenically marked naïve wild-type and P2rx7<sup>-/-</sup> OT-I T cells were infected orally with Lm-OVA. NAD was administered in the memory phase after infection to specifically deplete wild-type T<sub>RM</sub> cells. After two weeks, NAD-treated and NaCl-treated control mice were rechallenged orally with Lm-OVA and the secondary memory responses of wild-type and P2rx7<sup>-/-</sup> OT-I T cells were analyzed. **a–h**, The contribution of wild-type and P2rx7<sup>-/-</sup> OT-I T cells to the formation of secondary memory populations was analyzed in control and NAD-treated mice at >30 d post-Lm-OVA rechallenge. **a, c, e, g**, Representative flow cytometry plots show expression of the congenic markers CD45.1 and CD45.2 used to identify the contribution of wild-type (CD45.1<sup>+</sup>) and P2rx7<sup>-/-</sup> (CD45.2<sup>+</sup>) OT-I T cells to the formation of CD69<sup>+</sup> T<sub>RM</sub> cells in the SI-IELs (**a**), CD69<sup>+</sup> T<sub>RM</sub> cells in MLNs (**c**), KLRG1<sup>+</sup> T<sub>EM</sub> cells in the spleen (**e**) and CD62L<sup>+</sup> T<sub>CM</sub> cells in the spleen (**g**) under control conditions (left) and after NAD treatment (right). **b, d, f, h**, The ratio between wild-type and P2rx7<sup>-/-</sup> OT-I T cells was determined under control conditions and after NAD treatment for the CD69<sup>+</sup> T<sub>RM</sub> population of the liver and SI-IELs (**b**), the CD69<sup>+</sup> T<sub>RM</sub> population of the MLNs (**d**), the KLRG1<sup>+</sup> T<sub>EM</sub> population of the spleen and liver (**f**) and the CD62L<sup>+</sup> T<sub>CM</sub> population of the spleen and MLNs (**h**). Ratios were normalized to controls. Two-tailed Mann-Whitney *U*-test, \*\**P* < 0.01. Combined data from two independent experiments (*n* = 4 or 8 mice). The symbols represent individual mice; the bars represent the mean.

In this study, we found that T<sub>RM</sub> cells in the small intestine and liver expand and are maintained at elevated numbers after oral reinfection. Thus, reactivation appears to induce quantitative adaptations of local T<sub>RM</sub> populations. It remains to be determined if T<sub>RM</sub> cells retain indefinite capacity to repopulate their respective tissue after repeated antigen challenge. T<sub>RM</sub> cells might undergo further functional adaptations following reinfection, similar to their circulating counterparts<sup>18,19</sup>. Secondary T<sub>RM</sub> cells may thus differ from their primary counterparts in terms of quality, function and longevity.

Beyond nonlymphoid tissues, we found that oral reinfection drives the formation of secondary T<sub>RM</sub> cells in intestine-draining MLNs, but not in peripheral SLOs. Reactivated T<sub>RM</sub> cells from the skin and female reproductive tract can contribute to secondary T<sub>RM</sub> formation in draining lymph nodes<sup>15</sup>, thus suggesting that intestinal T<sub>RM</sub> cells may harbor similar potential. Indeed, specific ablation of T<sub>RM</sub> cells before reinfection strongly impaired secondary T<sub>RM</sub> formation in MLNs. Thus, pre-existing T<sub>RM</sub> cells in nonlymphoid tissues appear to be the main origin of secondary T<sub>RM</sub> development in draining SLOs. While the exact role of SLO T<sub>RM</sub> cells in host immune protection is unclear, these memory cells might contribute to the local immunosurveillance of SLOs<sup>15,42</sup>. Given their emergence in lymph nodes draining tissues frequently exposed to infections, SLO T<sub>RM</sub> cells may constitute an additional layer of immune protection.

While T<sub>RM</sub> cells share properties with effector T cells, including maintenance of direct effector functions and dependency on certain transcription factors<sup>12</sup>, they do not appear to be terminally differentiated. Instead, the T<sub>RM</sub>-dependent formation of SLO T<sub>RM</sub> cells beyond their tissue of residence suggests a certain degree of developmental plasticity. We found that T<sub>RM</sub> cells also maintain the capacity to form secondary T<sub>RM</sub> cells and differentiate into circulating KLRG1<sup>+</sup> T<sub>EM</sub> cells. Both liver and intestinal T<sub>RM</sub> cells formed

comparable circulating effector and memory responses following reactivation, indicating that the differentiation potential of T<sub>RM</sub> cells may be tissue-independent. Concordantly, a recent report demonstrated that reactivated intestinal T<sub>RM</sub> cells can acquire properties of circulating memory T cells<sup>43</sup>. Thus, T<sub>RM</sub> cells retain the potential to generate secondary responses in and beyond their respective tissue.

Tissue residency is regulated by the induction of adhesion molecules and the suppression of tissue exit pathways<sup>44</sup>. The formation of circulating ex-T<sub>RM</sub> cells implies downregulation of this tissue residency program in these memory cells. Hobit is a key regulator governing resident lymphocyte formation by restraining genes involved in tissue egress, including *Klf2* and *S1pr1* (ref. 9). Loss of Hobit expression may thus be crucial for T<sub>RM</sub> cells to exit their tissue and differentiate into circulating cells. Indeed, circulating ex-T<sub>RM</sub> cells had downregulated Hobit expression, did not express tissue retention molecules (for example, CD69) and acquired expression of molecules supporting tissue egress, including *Klf2* and *S1pr1*. Concordantly, Hobit downregulation appeared to be incompatible with maintaining a T<sub>RM</sub> phenotype. We found that antigen recognition resulted in rapid downregulation of Hobit by T<sub>RM</sub> cells, as previously observed in natural killer T cells and human effector CD8<sup>+</sup> T cells<sup>45,46</sup>. Antigen-driven loss of Hobit expression may thus relieve the suppression of exit pathways after reinfection and enable tissue egress of T<sub>RM</sub> cells.

Consecutive infections quantitatively and qualitatively shaped the circulating memory T cell pool, with a preferential accumulation of T<sub>EM</sub> cells at the expense of T<sub>CM</sub> features<sup>16–18,20,21</sup>. Interestingly, secondary and tertiary memory cells shared features with circulating ex-T<sub>RM</sub> cells, which primarily acquired a KLRG1<sup>+</sup> T<sub>EM</sub> phenotype. Reactivated T<sub>RM</sub> cells showed only limited potential to generate T<sub>CM</sub> cells, suggesting that T<sub>RM</sub> cells are not a main source of

secondary  $T_{CM}$  cells. Following adoptive transfer,  $T_{RM}$  cells exhibited limited proliferative capacity, in line with reported findings<sup>43</sup>, which may in part stem from the increased vulnerability of  $T_{RM}$  cells to ex vivo manipulation<sup>33,37,47</sup>. Selective depletion experiments demonstrated that  $T_{RM}$  cells considerably contributed to secondary  $T_{EM}$  formation after reinfection. While  $T_{CM}$  cells retained the capacity to form  $T_{RM}$  cells<sup>48,49</sup>, secondary  $T_{RM}$  cell development was largely dependent on pre-existing  $T_{RM}$  cells. Immunosurveillance of barrier tissues is primarily executed by local resident populations, despite abundant circulating memory T cells in the blood and SLOs<sup>10</sup>.  $T_{RM}$  cells are thus the first engaged memory T cell subset during reinfections where pathogens target epithelial surfaces; they initiate proliferation within days after antigen recognition<sup>13,14</sup>. Together with our findings, this suggests that reinfection at barrier sites induces rapid activation of local  $T_{RM}$  populations, which then substantially shape recall responses, both locally and systemically. We found that  $T_{RM}$ -derived circulating memory T cells exhibited distinct phenotypic features and improved protective ability compared to other  $T_{EM}$  populations. Tissue-specific imprints may consequently shape functional and migratory properties of circulating memory T cells after reinfection.

### Online content

Any methods, additional references, Nature Research reporting summaries, source data, extended data, supplementary information, acknowledgements, peer review information; details of author contributions and competing interests; and statements of data and code availability are available at <https://doi.org/10.1038/s41590-020-0723-4>.

Received: 4 November 2019; Accepted: 1 June 2020;

Published online: 13 July 2020

### References

- Lefrançois, L. Development, trafficking, and function of memory T-cell subsets. *Immunol. Rev.* **211**, 93–103 (2006).
- Mueller, S. N., Gebhardt, T., Carbone, F. R. & Heath, W. R. Memory T cell subsets, migration patterns, and tissue residence. *Annu. Rev. Immunol.* **31**, 137–161 (2013).
- Sallusto, F., Lenig, D., Förster, R., Lipp, M. & Lanzavecchia, A. Two subsets of memory T lymphocytes with distinct homing potentials and effector functions. *Nature* **401**, 708–712 (1999).
- Masopust, D., Vezys, V., Marzo, A. L. & Lefrançois, L. Preferential localization of effector memory cells in nonlymphoid tissue. *Science* **291**, 2413–2417 (2001).
- Wherry, E. J. et al. Lineage relationship and protective immunity of memory CD8 T cell subsets. *Nat. Immunol.* **4**, 225–234 (2003).
- Olson, J. A., McDonald-Hyman, C., Jameson, S. C. & Hamilton, S. E. Effector-like CD8<sup>+</sup> T cells in the memory population mediate potent protective immunity. *Immunity* **38**, 1250–1260 (2013).
- Sallusto, F., Geginat, J. & Lanzavecchia, A. Central memory and effector memory T cell subsets: function, generation, and maintenance. *Annu. Rev. Immunol.* **22**, 745–763 (2004).
- Mackay, L. K. et al. The developmental pathway for CD103<sup>+</sup>CD8<sup>+</sup> tissue-resident memory T cells of skin. *Nat. Immunol.* **14**, 1294–1301 (2013).
- Mackay, L. K. et al. Hobit and Blimp1 instruct a universal transcriptional program of tissue residency in lymphocytes. *Science* **352**, 459–463 (2016).
- Steinert, E. M. et al. Quantifying memory CD8 T cells reveals regionalization of immunosurveillance. *Cell* **161**, 737–749 (2015).
- Mueller, S. N. & Mackay, L. K. Tissue-resident memory T cells: local specialists in immune defence. *Nat. Rev. Immunol.* **16**, 79–89 (2016).
- Behr, F. M., Chuwonpad, A., Stark, R. & van Gisbergen, K. Armed and ready: transcriptional regulation of tissue-resident memory CD8 T cells. *Front. Immunol.* **9**, 1770 (2018).
- Park, S. L. et al. Local proliferation maintains a stable pool of tissue-resident memory T cells after antiviral recall responses. *Nat. Immunol.* **19**, 183–191 (2018).
- Beura, L. K. et al. Intravital mucosal imaging of CD8<sup>+</sup> resident memory T cells shows tissue-autonomous recall responses that amplify secondary memory. *Nat. Immunol.* **19**, 173–182 (2018).
- Beura, L. K. et al. T cells in nonlymphoid tissues give rise to lymph-node-resident memory T cells. *Immunity* **48**, 327–338.e5 (2018).
- Masopust, D., Ha, S.-J., Vezys, V. & Ahmed, R. Stimulation history dictates memory CD8 T cell phenotype: implications for prime-boost vaccination. *J. Immunol.* **177**, 831–839 (2006).
- Vezys, V. et al. Memory CD8 T-cell compartment grows in size with immunological experience. *Nature* **457**, 196–199 (2009).
- Jabbari, A. & Harty, J. T. Secondary memory CD8<sup>+</sup> T cells are more protective but slower to acquire a central-memory phenotype. *J. Exp. Med.* **203**, 919–932 (2006).
- Nolz, J. C. & Harty, J. T. Protective capacity of memory CD8<sup>+</sup> T cells is dictated by antigen exposure history and nature of the infection. *Immunity* **34**, 781–793 (2011).
- Fraser, K. A., Schenkel, J. M., Jameson, S. C., Vezys, V. & Masopust, D. Preexisting high frequencies of memory CD8<sup>+</sup> T cells favor rapid memory differentiation and preservation of proliferative potential upon boosting. *Immunity* **39**, 171–183 (2013).
- Van Braeckel-Budimir, N., Varga, S. M., Badovinac, V. P. & Harty, J. T. Repeated antigen exposure extends the durability of influenza-specific lung-resident memory CD8<sup>+</sup> T cells and heterosubtypic immunity. *Cell Rep.* **24**, 3374–3382.e3 (2018).
- Huster, K. M. et al. Unidirectional development of CD8<sup>+</sup> central memory T cells into protective *Listeria*-specific effector memory T cells. *Eur. J. Immunol.* **36**, 1453–1464 (2006).
- Graef, P. et al. Serial analysis of single-cell-derived immunocompetence reveals stemness of CD8<sup>+</sup> central memory T cells. *Immunity* **41**, 116–126 (2014).
- Masopust, D., Vezys, V., Wherry, E. J., Barber, D. L. & Ahmed, R. Cutting edge: gut microenvironment promotes differentiation of a unique memory CD8 T cell population. *J. Immunol.* **176**, 2079–2083 (2006).
- Sheridan, B. S. et al. Oral infection drives a distinct population of intestinal resident memory CD8<sup>+</sup> T cells with enhanced protective function. *Immunity* **40**, 747–757 (2014).
- van Stipdonk, M. J. B. et al. Dynamic programming of CD8<sup>+</sup> T lymphocyte responses. *Nat. Immunol.* **4**, 361–365 (2003).
- Joshi, N. S. et al. Inflammation directs memory precursor and short-lived effector CD8<sup>+</sup> T cell fates via the graded expression of T-bet transcription factor. *Immunity* **27**, 281–295 (2007).
- Sarkar, S. et al. Functional and genetic profiling of effector CD8 T cell subsets with distinct memory fates. *J. Exp. Med.* **205**, 625–640 (2008).
- Xin, A. et al. A molecular threshold for effector CD8<sup>+</sup> T cell differentiation controlled by transcription factors Blimp-1 and T-bet. *Nat. Immunol.* **17**, 422–432 (2016).
- Nishimura, M. et al. Dual functions of fractalkine/CX3C ligand 1 in trafficking of perforin<sup>+</sup>granzyme B<sup>+</sup> cytotoxic effector lymphocytes that are defined by CX3CR1 expression. *J. Immunol.* **168**, 6173–6180 (2002).
- Böttcher, J. P. et al. Functional classification of memory CD8<sup>+</sup> T cells by CX3CR1 expression. *Nat. Commun.* **6**, 8306 (2015).
- Gerlach, C. et al. The chemokine receptor CX3CR1 defines three antigen-experienced CD8 T cell subsets with distinct roles in immune surveillance and homeostasis. *Immunity* **45**, 1270–1284 (2016).
- Stark, R. et al.  $T_{RM}$  maintenance is regulated by tissue damage via P2RX7. *Sci. Immunol.* **3**, eaau1022 (2018).
- Skon, C. N. et al. Transcriptional downregulation of *S1pr1* is required for the establishment of resident memory CD8<sup>+</sup> T cells. *Nat. Immunol.* **14**, 1285–1293 (2013).
- Walzer, T. et al. Natural killer cell trafficking in vivo requires a dedicated sphingosine 1-phosphate receptor. *Nat. Immunol.* **8**, 1337–1344 (2007).
- Wirth, T. C. et al. Repetitive antigen stimulation induces stepwise transcriptome diversification but preserves a core signature of memory CD8<sup>+</sup> T cell differentiation. *Immunity* **33**, 128–140 (2010).
- Fernandez-Ruiz, D. et al. Liver-resident memory CD8<sup>+</sup> T cells form a frontline defense against malaria liver-stage infection. *Immunity* **45**, 889–902 (2016).
- Behr, F. M. et al. Blimp-1 rather than Hobit drives the formation of tissue-resident memory CD8<sup>+</sup> T cells in the lungs. *Front. Immunol.* **10**, 400 (2019).
- Schenkel, J. M., Fraser, K. A., Vezys, V. & Masopust, D. Sensing and alarm function of resident memory CD8<sup>+</sup> T cells. *Nat. Immunol.* **14**, 509–513 (2013).
- Schenkel, J. M. et al. Resident memory CD8 T cells trigger protective innate and adaptive immune responses. *Science* **346**, 98–101 (2014).
- Ariotti, S. et al. Skin-resident memory CD8<sup>+</sup> T cells trigger a state of tissue-wide pathogen alert. *Science* **346**, 101–105 (2014).
- Schenkel, J. M., Fraser, K. A. & Masopust, D. Cutting edge: resident memory CD8 T cells occupy frontline niches in secondary lymphoid organs. *J. Immunol.* **192**, 2961–2964 (2014).
- Fonseca, R. et al. Developmental plasticity allows outside-in immune responses by resident memory T cells. *Nat. Immunol.* **21**, 412–421 (2020).
- Schenkel, J. M. & Masopust, D. Tissue-resident memory T cells. *Immunity* **41**, 886–897 (2014).
- van Gisbergen, K. P. J. M. et al. Mouse Hobit is a homolog of the transcriptional repressor Blimp-1 that regulates NKT cell effector differentiation. *Nat. Immunol.* **13**, 864–871 (2012).

46. Kragten, N. A. M. et al. Blimp-1 induces and Hobit maintains the cytotoxic mediator granzyme B in CD8<sup>+</sup> T cells. *Eur. J. Immunol.* **48**, 1644–1662 (2018).
47. Wakim, L. M., Woodward-Davis, A. & Bevan, M. J. Memory T cells persisting within the brain after local infection show functional adaptations to their tissue of residence. *Proc. Natl Acad. Sci. USA* **107**, 17872–17879 (2010).
48. Enamorado, M. et al. Enhanced anti-tumour immunity requires the interplay between resident and circulating memory CD8<sup>+</sup> T cells. *Nat. Commun.* **8**, 16073 (2017).
49. Osborn, J. F. et al. Central memory CD8<sup>+</sup> T cells become CD69<sup>+</sup> tissue-residents during viral skin infection independent of CD62L-mediated lymph node surveillance. *PLoS Pathog.* **15**, e1007633 (2019).

**Publisher's note** Springer Nature remains neutral with regard to jurisdictional claims in published maps and institutional affiliations.

© The Author(s), under exclusive licence to Springer Nature America, Inc. 2020

## Methods

**Mice.** Wild-type CD45.2 (C57BL/6J) mice were purchased from Janvier Labs or bred in the animal facility of the Netherlands Cancer Institute. Wild-type CD45.1 (B6.SJL-*Ptprca*<sup>+/+</sup>*Peprca*<sup>+/+</sup>/BoyJ) mice, *P2rx7*<sup>-/-</sup> (B6.129P2-*P2rx7*<sup>tm1Gub/J</sup>) mice, OT-I (C57BL/6-Tg(Tcrb)1100Mjb/J) mice and ROSA26-*eYFP* (B6.129x1-*Gt(ROSA)26Sor*<sup>tm1(EYFP)Co/J</sup>) mice were purchased from The Jackson Laboratory and maintained in the animal facility of the Netherlands Cancer Institute. All mice were maintained under specific pathogen-free conditions. CD45.1 × CD45.2 mice were used as recipients throughout the study. Both female and male mice were used for this study and were aged between 8 and 16 weeks at the time of the experiments. For the adoptive transfer experiments, donor and recipient mice were sex-matched. Animals experiments were conducted according to institutional (Netherlands Cancer Institute) guidelines and the national guidelines of the Netherlands.

**Generation of Hobit reporter mice.** Hobit reporter (B6-Tg(Zfp683-tdTomato-P2A-Cre-P2A-DTR)) mice were generated in collaboration with Ozgene by inserting a targeting construct encoding for the fluorescent protein tdTomato, Cre recombinase and DTR (separated by P2A sequences) into the endogenous *Hobit* locus (Fig. 1a). Targeting was achieved via homologous recombination, whereby the targeting sequence replaced exons 2, 3 and 4, as well as intronic sequences of the *Hobit* locus (knockin knockout). The targeting sequence was cloned into a vector containing an *FRT*-flanked neomycin resistance gene (*neo*) and introduced into C57BL/6-derived embryonic stem cells. After selection with G418, correctly targeted clones were identified by PCR and injected into germline blastocysts to generate chimeric mice. Embryonic stem cell-derived offspring were then bred with FLPo-10 (B6.Cg-Tg(Pgk1-flpo)105Ykr/J) mice to remove *neo*.

**Infections, adoptive transfers and other in vivo treatments.** The spleens of CD45.1 Hobit reporter OT-I, CD45.2 Hobit reporter OT-I, CD45.2 Hobit reporter × ROSA26-*eYFP* OT-I, CD45.2 *P2rx7*<sup>-/-</sup> OT-I and CD45.1 wild-type OT-I mice were isolated and single-cell suspensions were generated by mechanical disruption. Naïve (CD44<sup>hi</sup>CD62L<sup>+</sup>) YFP<sup>-</sup>tdTomato<sup>-</sup> CD8<sup>+</sup> OT-I T cells were purified using a cell sorter (BD Biosciences) and 1 × 10<sup>4</sup> cells were transferred into recipient mice 1 d before infection. For competitive settings, naïve wild-type and *P2rx7*<sup>-/-</sup> OT-I T cells, or wild-type and Hobit reporter × ROSA26-*eYFP* OT-I T cells were mixed in a ratio of 1:1 and cotransferred. Mice were infected orally by feeding 2.5 × 10<sup>9</sup> (primary infection) or 2.5 × 10<sup>10</sup> (reinfection) colony-forming units (CFUs) of Lm-OVA InlA<sup>M</sup> (kindly provided by B. Sheridan, Stony Brook University) as described previously<sup>25</sup>. To trigger P2RX7 and deplete wild-type T<sub>RM</sub> cells in vivo, mice were injected intravenously with 60 mg of NAD<sup>+</sup> (Sigma-Aldrich) in 0.9% NaCl (pH 6.0) or with 0.9% NaCl as the control. To selectively deplete Hobit<sup>+</sup> Hobit reporter × ROSA26-*eYFP* OT-I T<sub>RM</sub> cells in vivo, mice were injected intraperitoneally with 400 ng DT (Merck) in PBS or with PBS as the control for 4 consecutive days. At the indicated time points after infection, mice were killed and tissues were collected for analysis of OT-I T cell responses.

For the adoptive transfer experiments with polyclonal memory CD8<sup>+</sup> T cells, wild-type CD45.1 and CD45.2 mice were infected intraperitoneally with 1 × 10<sup>8</sup> plaque-forming units (PFUs) of LCMV (Armstrong). In the memory phase after infection, CD8<sup>+</sup>TCRγδ<sup>-</sup>CD44<sup>hi</sup>CD69<sup>-</sup>CD62L<sup>+</sup> T<sub>CM</sub> cells from the spleen and CD8<sup>+</sup>TCRγδ<sup>-</sup>CD69<sup>+</sup>CD62L<sup>-</sup> T<sub>RM</sub> cells from the liver or SI-IELs were purified using a cell sorter. To preserve T<sub>RM</sub> cell viability, donor mice were injected intraperitoneally with 50 μg of ARTC2.2-blocking nanobody s+16a (BioLegend) 30 min before mice were killed<sup>33,37</sup>. For cotransfers, the frequency of D<sup>b</sup>GP33<sup>+</sup> cells in purified donor populations was determined and donor cells were mixed to achieve a ratio of 1:1 in the D<sup>b</sup>GP33<sup>+</sup> population. Recipient mice were injected with 2–4 × 10<sup>5</sup> D<sup>b</sup>GP33<sup>+</sup> cells per donor population intravenously and infected intraperitoneally with 1 × 10<sup>8</sup> PFUs of LCMV (Armstrong) 2 weeks after transfer. At the indicated time points after infection, mice were killed and tissues were collected for analysis of donor CD8<sup>+</sup> T cell responses.

For the adoptive transfer experiments with memory OT-I T cells, mice containing naïve CD45.1 and CD45.2 Hobit reporter OT-I T cells were infected orally with 2.5 × 10<sup>9</sup> CFUs of Lm-OVA InlA<sup>M</sup>. In the memory phase after infection, CD45.1<sup>+</sup>/CD45.2<sup>+</sup>CD8<sup>+</sup>CD69<sup>-</sup>CD62L<sup>+</sup> OT-I T<sub>CM</sub> cells from the spleen and CD45.1<sup>+</sup>/CD45.2<sup>+</sup>CD8<sup>+</sup>CD69<sup>+</sup>CD62L<sup>-</sup> OT-I T<sub>RM</sub> cells from SI-IELs were purified using a cell sorter. To preserve T<sub>RM</sub> cell viability, donor mice were injected intraperitoneally with 50 μg of ARTC2.2-blocking nanobody s+16a 30 min before being killed<sup>33,37</sup>. Equal numbers of OT-I T<sub>CM</sub> and T<sub>RM</sub> cells were cotransferred. Recipient mice were injected with 2–3 × 10<sup>4</sup> OT-I cells per donor population intravenously and infected orally with 2.5 × 10<sup>10</sup> CFUs of Lm-OVA InlA<sup>M</sup> 2 weeks after transfer. At the indicated time points after infection, mice were killed and tissues were collected for analysis of donor OT-I T cell responses.

To determine the protective capacity of secondary memory OT-I T cell subsets, mice containing naïve Hobit reporter × ROSA26-*eYFP* OT-I T cells were infected orally with 2.5 × 10<sup>9</sup> CFUs of Lm-OVA InlA<sup>M</sup>; >30 d later, they were reinfected with 2.5 × 10<sup>10</sup> CFUs of Lm-OVA InlA<sup>M</sup>. In the memory phase after reinfection, CD45.2<sup>+</sup>CD8<sup>+</sup>CD62L<sup>-</sup>YFP<sup>+</sup> and YFP<sup>-</sup> OT-I T<sub>EM</sub> cells from the spleen were purified using a cell sorter. Recipient mice were injected with 7 × 10<sup>4</sup> cells intravenously and infected orally with 2.5 × 10<sup>10</sup> CFUs of Lm-OVA InlA<sup>M</sup> 1 d later. At the indicated

time points after infection, single-cell suspensions of tissues were incubated with 1% saponin for 1–2 h at 4 °C. Tissue homogenates were plated on Brain Heart Infusion Agar plates supplemented with 50 μg ml<sup>-1</sup> streptomycin. Colonies were counted after 1 d at 37 °C.

**Isolation of lymphocytes from tissues.** Single-cell suspensions from the spleen, lymph nodes and liver were prepared by mechanical disruption by passing over a 70-μm cell strainer. SI-LPL and SI-IELs were prepared from the small intestine. After removal of residual fat tissue, Peyer's patches and feces, the small intestine tissue was cut into smaller pieces and incubated in Hanks' Balanced Salt Solution (Gibco) with 10% FCS, 5 mM of EDTA and 1 mM of dithiothreitol for 30 min at 37 °C and vortexed repeatedly. The SI-IEL fraction was isolated by filtering over a 70-μm cell strainer. To isolate the SI-LPL fraction, SI-IEL-depleted intestine pieces were washed in Hanks' Balanced Salt Solution supplemented with 2% FCS and enzymatically digested for 30 min at 37 °C with 375 U ml<sup>-1</sup> Collagenase type I (Worthington) and 0.15 mg ml<sup>-1</sup> DNase I (grade II, bovine pancreas; Roche) in Roswell Park Memorial Institute 1640 medium (supplemented with 10% FCS). Single-cell suspensions were generated by filtering over a 70-μm cell strainer. The isolated lymphocytes from the liver, SI-IELs and SI-LPL were purified by density centrifugation on a 66 and 44% Percoll gradient (GE Healthcare). Contaminating erythrocytes were removed using red blood cell lysis buffer (155 mM of NH<sub>4</sub>Cl, 10 mM of KHCO<sub>3</sub>, 0.1 mM of EDTA).

**In vitro stimulation.** OT-I T cells were isolated from tissues as described earlier and cultured in vitro in Roswell Park Memorial Institute 1640 medium (Gibco) supplemented with 10% (v/v) FCS (Bodging BV), 100 U ml<sup>-1</sup> penicillin (Sigma-Aldrich), 100 μg ml<sup>-1</sup> streptomycin (Sigma-Aldrich), 2 mM of L-glutamine (Sigma-Aldrich) and 55 μM 2-Mercaptoethanol (Gibco). OT-I T cells were stimulated by coculture with preseeded MEC.B7.SigOVA cells for 20 h, as described previously<sup>26</sup>.

**Flow cytometry.** Cells were incubated with antibodies and tetramers for 25 min at 4 °C in the dark and washed with PBS (supplemented with 0.5% (v/v) FCS). Antibodies were purchased from BioLegend, eBioscience, BD Biosciences or BD Pharmingen. All antibodies used are listed in Supplementary Table 1 and in the Nature Research Reporting Summary linked to this article. H-2 D<sup>b</sup>/KAVYNFATC (GP33) tetramers were kindly provided by R. Arens (Leiden University Medical Center). Exclusion of dead cells was performed with LIVE/DEAD Fixable Near-IR Dead Cell Stain Kit (Thermo Fisher Scientific). To stain intracellular molecules, the Foxp3/Transcription Factor Staining Buffer Set (eBioscience) was used according to the manufacturer's specifications. Samples were acquired on LSRFortessa and FACSymphony flow cytometers (BD Biosciences) using the BD FACSDiva software v9.0 (BD Biosciences); data were analyzed using the FlowJo v10 software (FlowJo, LLC). Cell sorting was performed using the BD FACSAria III sorter (BD Biosciences).

**Quantitative PCR with reverse transcription (qRT-PCR) analysis.** RNA was isolated using the TRIzol Reagent (Invitrogen). Complementary DNA (cDNA) synthesis was performed on a Verity 96-well Fast Thermo Cyclor (Applied Biosystems) using the iScript RT-PCR Kit (Bio-Rad Laboratories). Quantitative PCR was performed on a StepOnePlus System (Applied Biosystems) using the Fast SYBR Green Master Mix (Thermo Fisher Scientific). The following primer sets were used: murine *Hobit* (forward: 5'-TCCTCCCACTCTCATCTCCAA-3'; reverse: 5'-CAGACCCACTGGCTGTTCAT-3'); *Hprt* (forward: 5'-TGAAGAGCTA CTGTAATGATCAGTCAAC-3'; reverse: 5'-AGCAAGCTTGCAACCTTAAC CA-3'). Values are represented relative to that of *HPRT1* (*HPRT*) and calibrated relative to naïve CD8<sup>+</sup> T cells unless indicated otherwise.

**RNA-seq analysis.** Primary and secondary memory Hobit reporter × ROSA26-*eYFP* OT-I T cell subsets were isolated by fluorescence-activated cell sorting (FACS) from the spleen, liver and small intestine (SI-IELs and SI-LPL combined) of mice previously infected with Lm-OVA. T<sub>CM</sub> (CD69<sup>-</sup>CD62L<sup>+</sup>) and T<sub>EM</sub> cells (CD69<sup>+</sup>CD62L<sup>-</sup>) were isolated from the spleen; T<sub>RM</sub> cells (CD69<sup>+</sup>CD62L<sup>-</sup>tdTomato<sup>+</sup>) were isolated from the liver and small intestine. Naïve (CD44<sup>hi</sup>CD62L<sup>+</sup>) Hobit reporter × ROSA26-*eYFP* OT-I T cells were isolated from the spleen of naïve mice. Sequencing was performed at Single Cell Discoveries (Utrecht, the Netherlands). In brief, total RNA was extracted using the standard TRIzol protocol and used for library preparation and sequencing. mRNA was processed as described previously, following an adapted version of the single-cell mRNA sequencing protocol of Cell Expression by Linear amplification and Sequencing (CEL-Seq)<sup>50,51</sup>. Samples were barcoded with CEL-Seq primers during reverse transcription and pooled after second strand synthesis. The resulting cDNA was amplified with an overnight in vitro transcription reaction. From this amplified RNA, sequencing libraries were prepared with Illumina TruSeq small RNA primers. Paired-end sequencing was performed on the Illumina NextSeq500 platform. Three biological replicates were sequenced for each sample. Read 1 was used to identify the Illumina library index and CEL-Seq sample barcode. Read 2 was aligned to the mm10 mouse refSeq transcriptome using the Burrows-Wheeler Aligner v0.7.17 (ref. <sup>52</sup>). Reads that mapped equally well to multiple locations were discarded. Mapping and generation

of count tables were done using the MapAndGo2 script. Samples were normalized using reads per million normalization. Genes were selected for differential expression analysis when three or more samples reported more than three counts per million. Differential expression analysis was performed in R v.3.5.0 using the edgeR v.3.24.3 and limma v.3.38.3 Bioconductor packages<sup>53,54</sup>. Differentially expressed genes were selected using a false discovery rate (FDR) (Benjamini–Hochberg) cutoff of 0.05. Volcano plots were visualized with the EnhancedVolcano v.1.2.0 package (<https://github.com/kevinblighe/EnhancedVolcano>).

**Statistical analysis.** Statistical analysis was carried out using Prism v.8 (GraphPad Software). The tests used are indicated in the figure legends. Unless otherwise indicated, differences were not statistically significant.  $P < 0.05$  was considered statistically significant (\* $P < 0.05$ ; \*\* $P < 0.01$ ; \*\*\* $P < 0.001$ ).

**Reporting Summary.** Further information on research design is available in the Nature Research Reporting Summary linked to this article.

### Data availability

The data that support the findings of this study are available from the corresponding author upon reasonable request. The RNA-seq data have been deposited at the National Center for Biotechnology Information Sequence Read Archive under the BioProject accession code [PRJNA635759](https://www.ncbi.nlm.nih.gov/bioproject/PRJNA635759).

### References

50. Hashimshony, T., Wagner, F., Sher, N. & Yanai, I. CEL-Seq: single-cell RNA-seq by multiplexed linear amplification. *Cell Rep.* **2**, 666–673 (2012).
51. Simmini, S. et al. Transformation of intestinal stem cells into gastric stem cells on loss of transcription factor Cdx2. *Nat. Commun.* **5**, 5728 (2014).
52. Li, H. & Durbin, R. Fast and accurate long-read alignment with Burrows–Wheeler transform. *Bioinformatics* **26**, 589–595 (2010).
53. Robinson, M. D., McCarthy, D. J. & Smyth, G. K. edgeR: a Bioconductor package for differential expression analysis of digital gene expression data. *Bioinformatics* **26**, 139–140 (2010).
54. Ritchie, M. E. et al. *limma* powers differential expression analyses for RNA-sequencing and microarray studies. *Nucleic Acids Res.* **43**, e47 (2015).

### Acknowledgements

We thank members of the van Gisbergen laboratory and Department of Hematopoiesis, as well as M. Wolkers, for fruitful discussions. F.M.B., L.P.V. and K.P.J.M.v.G. were supported by Vidi grant no. 917.13.338 from the Netherlands Organization for Scientific Research (NWO) and a fellowship from the Landsteiner Foundation of Blood Transfusion Research. R.S. was supported by a fellowship from the Alexander von Humboldt Foundation and by Veni grant no. 016.186.116 from the (NWO).

### Author contributions

F.M.B., R.A.W.v.L., R.S. and K.P.J.M.v.G. designed the experiments. F.M.B., L.P.V., N.A.M.K. and R.S. performed the experiments. T.H.W., B.S.S. and R.A. contributed critical reagents and experimental help. F.M.B. analyzed the data and performed the statistical analysis. T.J.P.v.D. analyzed the RNA-seq data. F.M.B. and K.P.J.M.v.G. wrote the manuscript.

### Competing interests

The authors declare no competing interests.

### Additional information

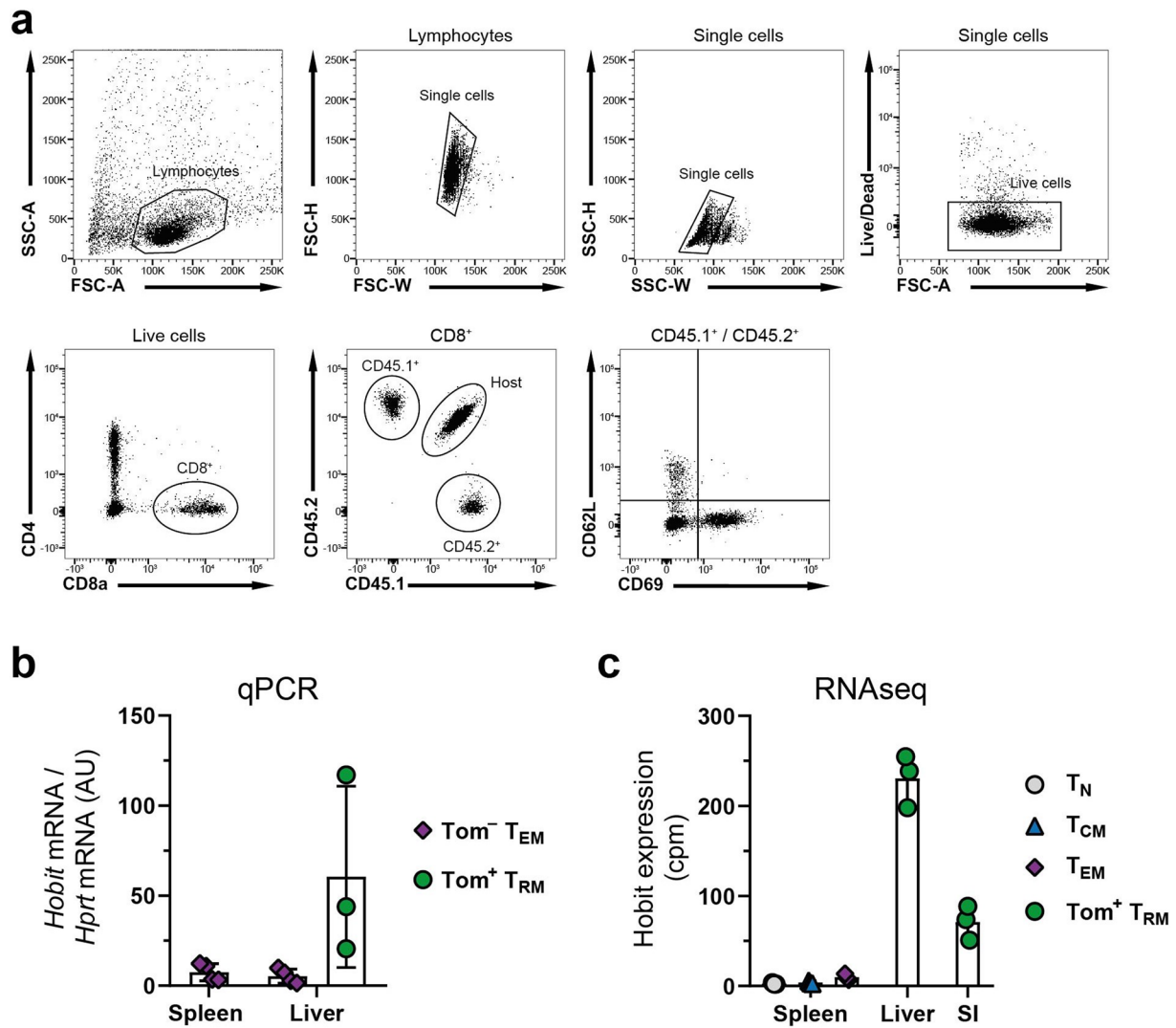
**Extended data** is available for this paper at <https://doi.org/10.1038/s41590-020-0723-4>.

**Supplementary information** is available for this paper at <https://doi.org/10.1038/s41590-020-0723-4>.

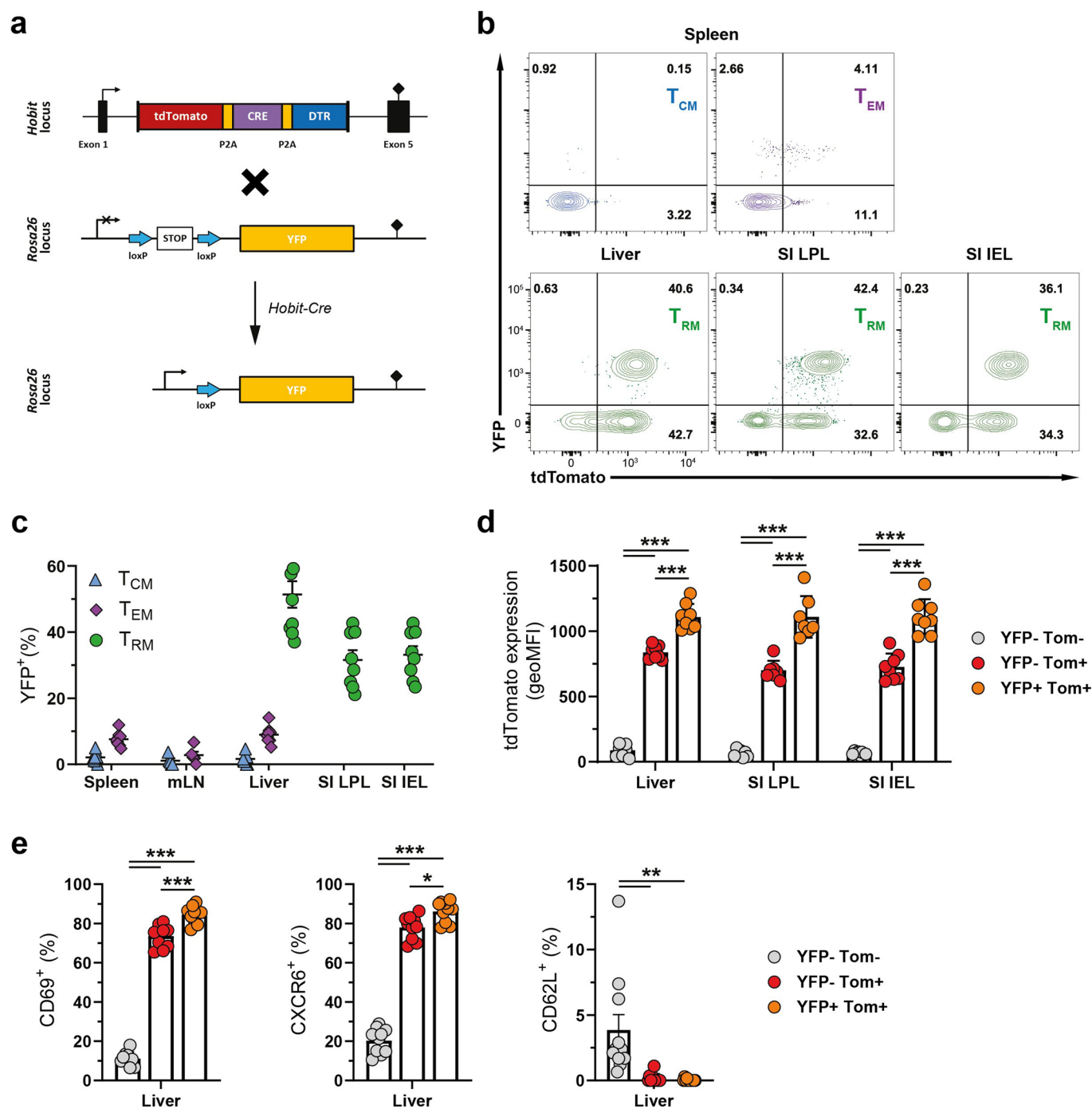
**Correspondence and requests for materials** should be addressed to K.P.J.M.v.G.

**Reprints and permissions information** is available at [www.nature.com/reprints](http://www.nature.com/reprints).

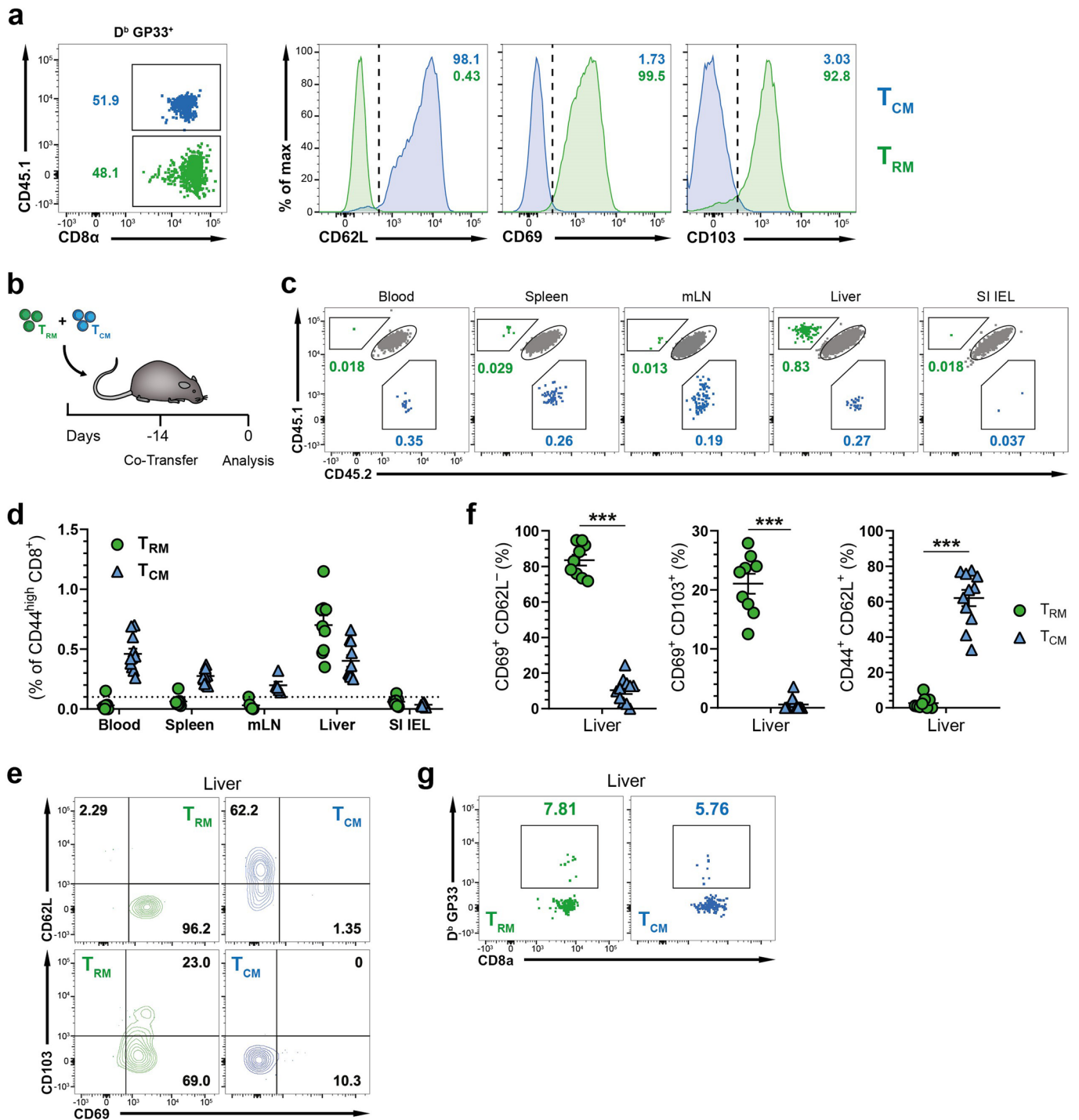
**Editor recognition statement** L. A. Dempsey was the primary editor on this article and managed its editorial process and peer review in collaboration with the rest of the editorial team.



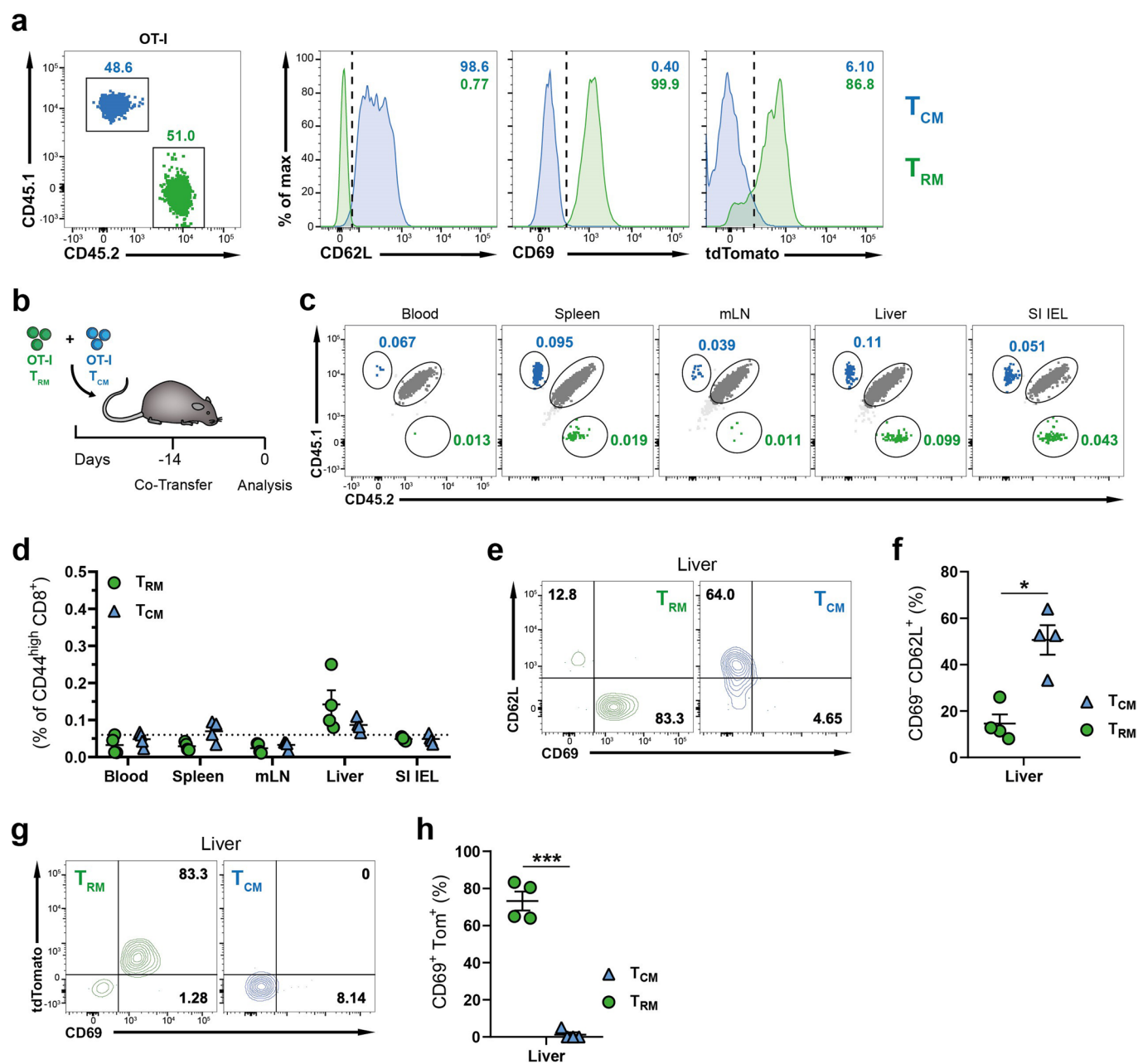
**Extended Data Fig. 1 | Expression of reporter protein tdTomato reflects *Hobit* expression.** **a**, Exemplary gating strategy for the analysis of OT-I T cells. **b**, **c**, HR × *Rosa26<sup>eYFP</sup>* naïve and memory OT-I T cells were FACS-purified from spleen liver and small intestine at >30 days after oral infection with *L.m.*-OVA. The expression of *Hobit* mRNA in CD44<sup>lo</sup> CD62L<sup>+</sup> T<sub>N</sub> cells, CD69<sup>-</sup> CD62L<sup>+</sup> T<sub>CM</sub> cells, tdTomato<sup>-</sup> (Tom<sup>-</sup>) CD69<sup>-</sup> CD62L<sup>-</sup> T<sub>EM</sub> cells from spleen and liver, and tdTomato<sup>+</sup> (Tom<sup>+</sup>) CD69<sup>+</sup> CD62L<sup>-</sup> T<sub>RM</sub> cells from liver and small intestine (SI, SI LPL and SI LPL combined) was determined via **(b)** qPCR and via **(c)** RNA sequencing. Combined data from two independent experiments (n=3 or 4 biological replicates) **(b)** and data from one experiment (n=3 biological replicates) **(c)**. Symbols represent biological replicates; bars represent the mean. Error bars represent mean ± SD.



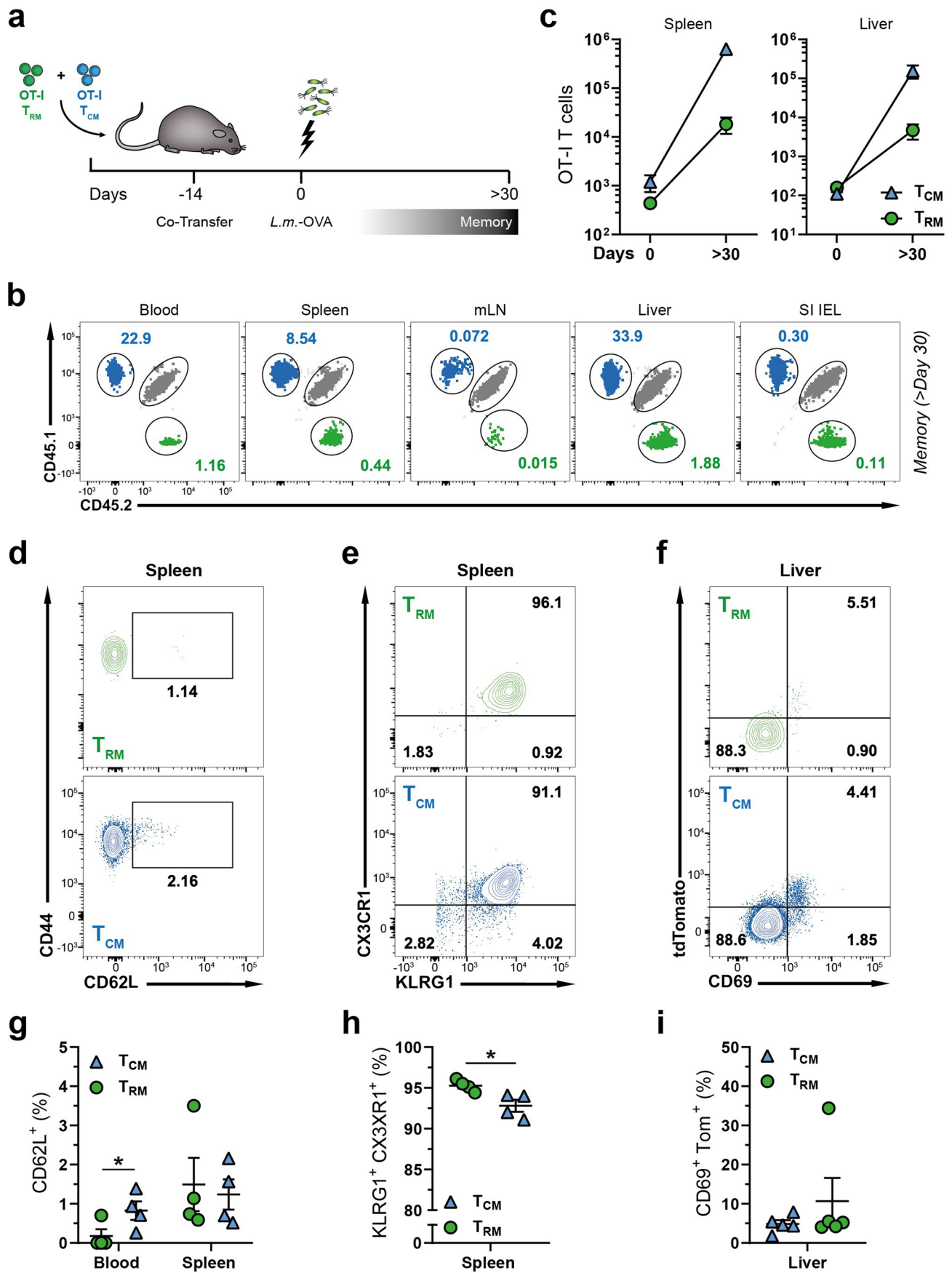
**Extended Data Fig. 2 | Fate-mapping of Hobit-expressing cells identifies primary  $T_{RM}$  cells.** **a**, Schematic representation is shown of the experimental setup using HR OT-I mice crossed onto *Rosa26-flox-STOP-flox-eYFP* (*Rosa26<sup>eYFP</sup>*) reporter mice for fate mapping of  $T_{RM}$  cells during secondary responses. **(b–e)** The phenotype of adoptively transferred HR × *Rosa26<sup>eYFP</sup>* OT-I T cells was analyzed at >30 days after oral infection with *L.m.*-OVA. **b**, Representative flow cytometry plots show expression of YFP and tdTomato by  $T_{CM}$  (CD69<sup>+</sup> CD62L<sup>+</sup>) and  $T_{EM}$  (CD69<sup>+</sup> CD62L<sup>-</sup>) cells in spleen, and  $T_{RM}$  cells (CD69<sup>+</sup> CD62L<sup>-</sup>) in liver, SI IEL and LPL. **c**, The frequency of YFP<sup>+</sup> expression was quantified within the indicated populations of memory HR × *Rosa26<sup>eYFP</sup>* OT-I T cells. **d**, The expression levels (geoMFI) of tdTomato within the indicated populations of memory HR × *Rosa26<sup>eYFP</sup>* OT-I T cells were quantified. Two-way ANOVA with Tukey’s multiple comparisons test, \*\*\* $P < 0.0001$ . **e**, The frequencies of CD69<sup>+</sup>, CXCR6<sup>+</sup> and CD62L<sup>+</sup> expression within the indicated populations was quantified. One-way ANOVA with Tukey’s multiple comparisons test, \* $P = 0.0131$ , \*\*\* $P < 0.01$ , \*\*\* $P < 0.0001$ . Combined data is shown from two independent experiments ( $n = 8$  or 11 mice). Symbols represent individual mice; bars represent the mean. Error bars represent mean ± SEM.



**Extended Data Fig. 3 | Polyclonal donor  $T_{RM}$  cells maintain resident phenotype after adoptive transfer.** Congenically marked  $T_{RM}$  (green) and  $T_{CM}$  cells (blue), that were FACS-purified from SI IEL and spleen of LCMV-infected mice, respectively, were co-transferred into naïve recipients, and distribution and phenotype of donor cells were analyzed 14 days later. **a**, Dot plot shows distribution of  $T_{RM}$  and  $T_{CM}$  cells within virus-specific ( $D^b$  GP33<sup>+</sup>) donor cell population (left panel) and histograms display expression of phenotypic markers by  $D^b$  GP33<sup>+</sup>  $T_{RM}$  and  $T_{CM}$  cells (right panel) prior to transfer. **b**, Graphic scheme depicts setting of adoptive transfer experiments. **c**, Representative flow cytometry plots show expression of the congenic markers CD45.1 and CD45.2 to identify donor  $T_{RM}$ -derived (green), donor  $T_{CM}$ -derived (blue) and host-derived (grey) cells within the memory (CD44<sup>high</sup>) CD8<sup>+</sup> T cell population in the indicated tissues at two weeks after transfer. **d**, The frequency of  $T_{RM}$ - and  $T_{CM}$ -derived CD44<sup>high</sup> cells was determined in indicated tissues. Dotted line indicates detection limit, as determined by analysis of non-transferred mice. **e**, Representative flow cytometry plots show expression of CD62L, CD69 and CD103 on CD44<sup>high</sup>  $T_{RM}$  and  $T_{CM}$  donor cells in liver. **f**, The frequency of CD69<sup>+</sup> CD62L<sup>-</sup>, CD69<sup>+</sup> CD103<sup>+</sup> and CD44<sup>+</sup> CD62L<sup>+</sup> cells within the donor populations was quantified. Two-tailed paired *t*-test, \*\*\**P* < 0.001. **g**, Representative flow cytometry plots show presence of virus-specific ( $D^b$  GP33<sup>+</sup>) cells within donor populations in the liver. Combined data is shown from two independent experiments (*n* = 9 or 11 mice). Symbols represent individual mice; bars represent the mean. Error bars represent mean  $\pm$  SEM.

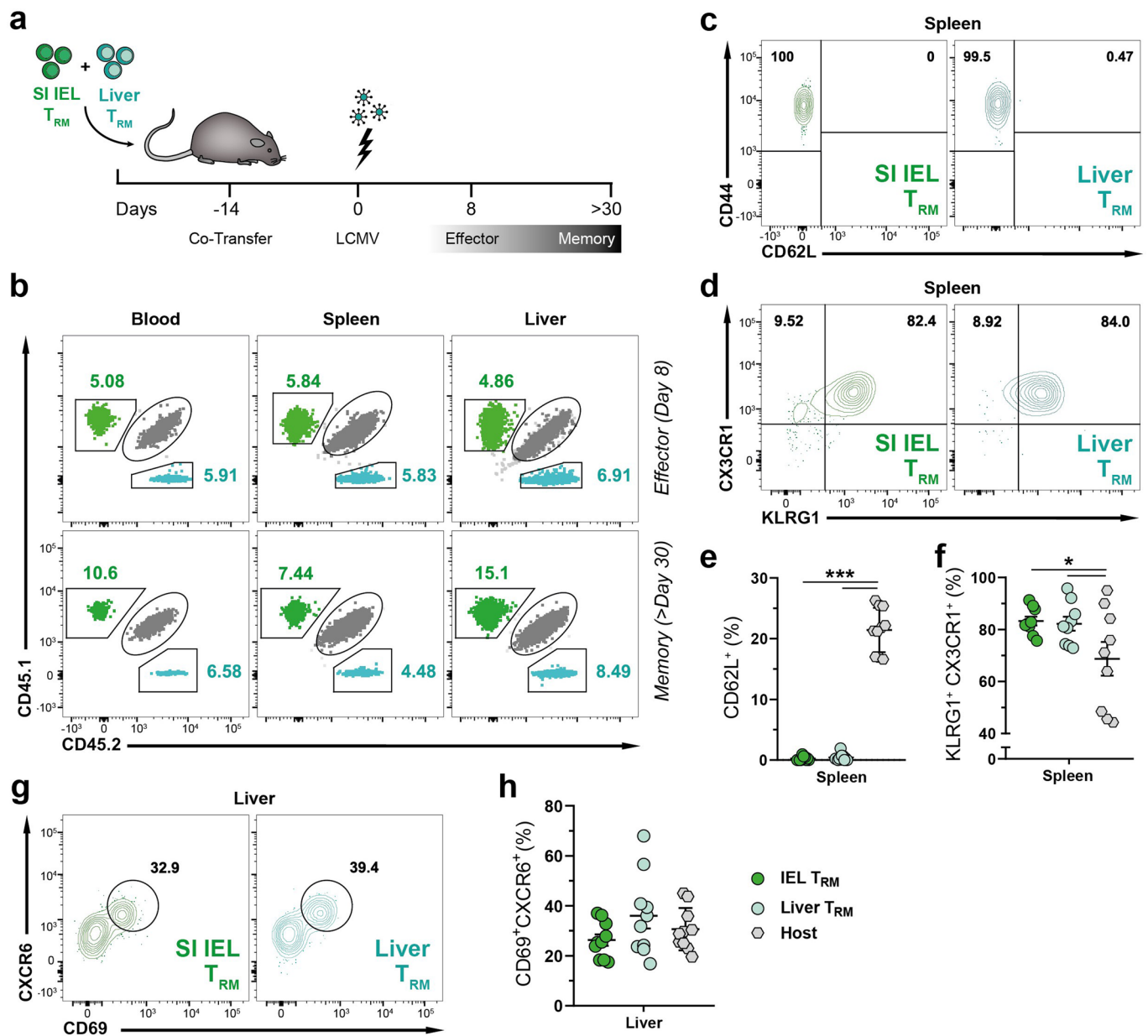


**Extended Data Fig. 4 | Monoclonal donor  $T_{RM}$  cells maintain resident phenotype after adoptive transfer.** Congenically marked HR OT-I  $T_{RM}$  (green) and HR OT-I  $T_{CM}$  cells (blue), that were FACS-purified from SI IEL and spleen of *L.m.*-OVA -infected mice, respectively, were co-transferred into naïve recipients, and distribution and phenotype of donor cells were analyzed 14 days later. **a**, Dot plot shows distribution of HR OT-I  $T_{RM}$  and  $T_{CM}$  cells within the total donor cell population (left panel) and histograms display expression of phenotypic markers by OT-I  $T_{RM}$  and  $T_{CM}$  cells (right panel) prior to transfer. **b**, Graphic scheme depicts setting of adoptive transfer experiments. **c**, Representative flow cytometry plots show expression of the congenic markers CD45.1 and CD45.2 to identify donor  $T_{RM}$ -derived (green), donor  $T_{CM}$ -derived (blue) and host-derived (grey) cells within the memory ( $CD44^{high}$ )  $CD8^{+}$  T cell population in the indicated tissues at two weeks after transfer. **d**, The frequency of  $T_{RM}$ - and  $T_{CM}$ -derived  $CD44^{high} CD8^{+}$  cells was determined in indicated tissues. Dotted line indicates detection limit, as determined by analysis of non-transferred mice. **e**, Representative flow cytometry plots show expression of CD62L and CD69 on  $CD44^{high} T_{RM}$  and  $T_{CM}$  donor cells in liver. **f**, The frequency of  $CD69^{-} CD62L^{+}$  cells within the donor populations was quantified. Two-tailed paired *t*-test,  $*P=0.0173$ . **g**, Representative flow cytometry plots show expression of tdTomato and CD69 on  $CD44^{high} T_{RM}$  and  $T_{CM}$  donor cells in liver. **h**, The frequency of  $CD69^{+} tdTomato^{+}$  cells within the donor populations was quantified. Two-tailed paired *t*-test,  $***P=0.0005$ . Combined data from two independent experiments ( $n=4$  mice). Symbols represent individual mice; bars represent the mean. Error bars represent mean  $\pm$  SEM.

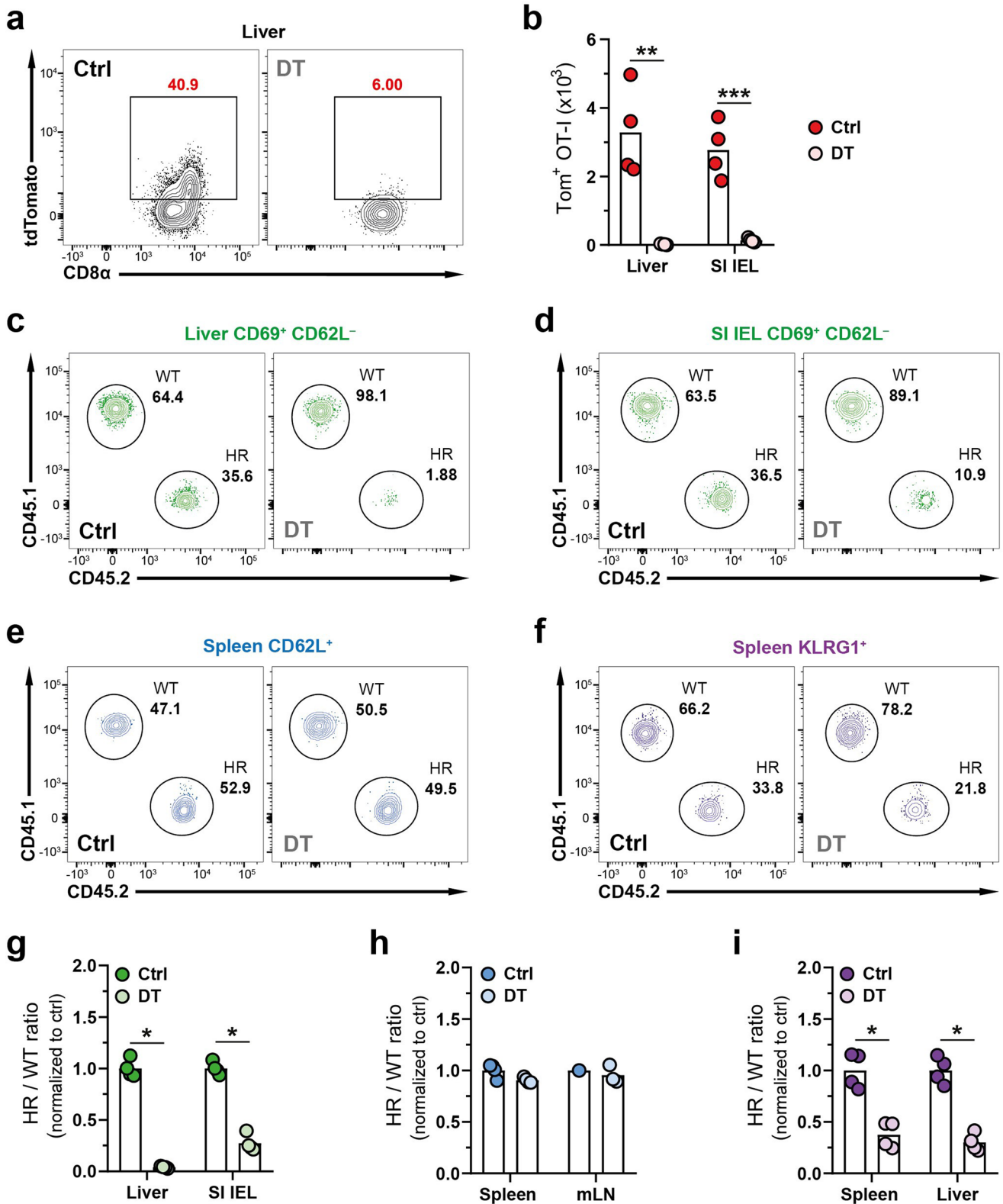


Extended Data Fig. 5 | See next page for caption.

**Extended Data Fig. 5 | Monoclonal CD8<sup>+</sup> T<sub>RM</sub> cells generate systemic responses upon pathogen rechallenge.** **a**, Graphic scheme depicts settings of rechallenge experiments with adoptively transferred HR OT-I T<sub>CM</sub> and T<sub>RM</sub> cells. In brief, congenically marked HR OT-I T<sub>RM</sub> and T<sub>CM</sub> cells were FACS-purified from SI IEL and spleen of *L.m.*-OVA -infected mice, respectively, and co-transferred into naïve recipients, which were challenged orally with *L.m.*-OVA 14 days later. The offspring of the donor OT-I T cells was analyzed at >30 days p.i. **b**, Representative flow cytometry plots show expression of the congenic markers CD45.1 and CD45.2 to identify donor T<sub>RM</sub>-derived (green), donor T<sub>CM</sub>-derived (blue) and host-derived (grey) cells within the CD8<sup>+</sup> T cell population in the indicated tissues at >30 days p.i. **c**, The number of T<sub>RM</sub>- and T<sub>CM</sub>-derived OT-I T cells was determined in spleen and liver at the indicated time points before and after *L.m.*-OVA challenge. **(d-f)** Representative flow cytometry plots show **(d)** expression of CD62L and CD44 and **(e)** CX3CR1 and KLRG1 on HR OT-I T<sub>RM</sub>- and T<sub>CM</sub>-derived memory T cells in spleen, and **(f)** expression of tdTomato and CD69 by HR OT-I T<sub>RM</sub>- and T<sub>CM</sub>-derived memory T cells in liver at >30 days after *L.m.*-OVA challenge. **(g-i)** The frequency of **(g)** CD62L expression, **(h)** KLRG1 and CX3CR1 co-expression and **(i)** CD69 and tdTomato co-expression within the offspring of donor T<sub>RM</sub> and T<sub>CM</sub> populations was quantified. Two-tailed paired *t*-test, \**P*=0.0195 **(g)**, \**P*=0.0241 **(h)**. Combined data from two independent experiments (*n*=4 or 5 mice). Symbols represent the mean **(c)** or individual mice **(g-i)**; bars represent the mean. Error bars represent mean ± SEM.

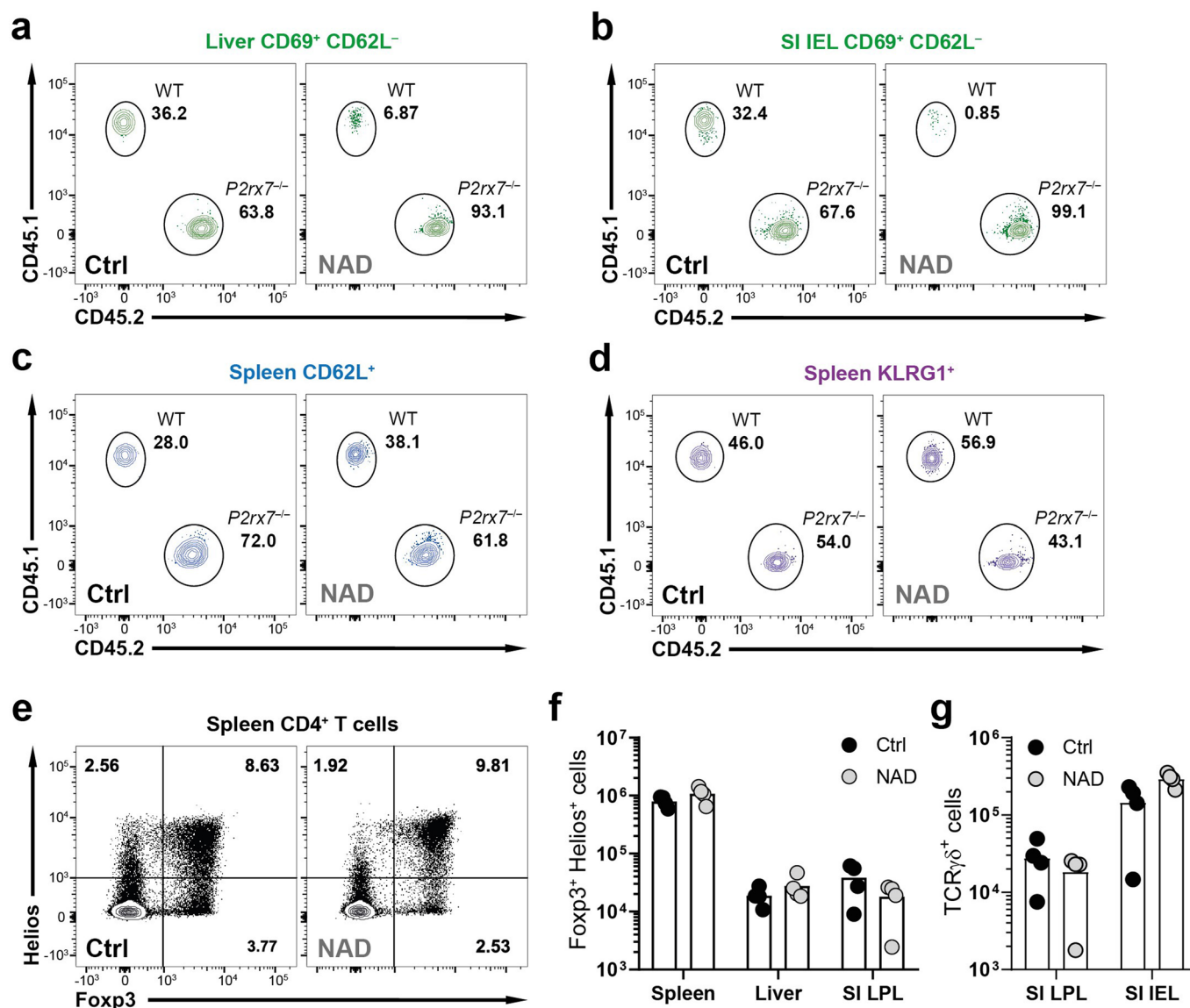


**Extended Data Fig. 6 | Intestinal and liver CD8<sup>+</sup>  $T_{RM}$  cells generate systemic responses upon pathogen rechallenge.** **a**, Graphic scheme depicts settings of rechallenge experiments with adoptively transferred  $T_{RM}$  cells from liver and intestine. In brief, congenically marked  $T_{RM}$  cells were FACS-purified from liver and SI IEL of LCMV-infected mice, respectively, and co-transferred into naïve recipients, which were challenged with LCMV two weeks later. The offspring of the virus-specific ( $D^b$  GP33<sup>+</sup>) donor T cells was analyzed at 8 and >30 days p.i. **b**, Representative flow cytometry plots show expression of the congenic markers CD45.1 and CD45.2 to identify donor SI IEL  $T_{RM}$ -derived (green), donor liver  $T_{RM}$ -derived (turquoise) and host-derived (grey) cells within the  $D^b$  GP33<sup>+</sup> T cell population in the indicated tissues at 8 and >30 days p.i. **c, d**, Representative flow cytometry plots show (**c**) expression of CD44 and CD62L and (**d**) expression of CX3CR1 and KLRG1 on  $D^b$  GP33<sup>+</sup> SI IEL  $T_{RM}$ - (left) and liver  $T_{RM}$ -derived memory T cells (right) in spleen at >30 days after LCMV challenge. **e, f**, The frequency of (**e**) CD62L expression and (**f**) co-expression of KLRG1 and CX3CR1 within the offspring of donor  $T_{RM}$  populations and host  $D^b$  GP33<sup>+</sup> cells were quantified. Two-tailed paired *t*-test, \**P* < 0.05; \*\*\**P* < 0.001. **g**, Representative flow cytometry plots show expression of CXCR6 and CD69 on  $D^b$  GP33<sup>+</sup> secondary memory cells developing from donor SI IEL  $T_{RM}$  (left) or liver  $T_{RM}$  (right) cells after LCMV challenge. **h**, The frequency of  $T_{RM}$  cells (CD69<sup>+</sup> CXCR6<sup>+</sup>) within the donor populations was quantified. Two-tailed paired *t*-test. Combined data from two independent experiments (*n* = 9 or 10 mice). Symbols represent individual mice; bars represent the mean. Error bars represent mean ± SEM.



Extended Data Fig. 7 | See next page for caption.

**Extended Data Fig. 7 | Efficient depletion of T<sub>RM</sub> cells by DT administration.** Wild-type mice containing congenically marked naïve WT and HR OT-I T cells were infected orally with *L.m.*-OVA. DT was administered in the memory phase after infection to specifically deplete HR T<sub>RM</sub> cells. One day after the last DT administration, presence and phenotype of donor WT and HR OT-I T cells were analyzed. **a**, Representative flow cytometry plots show expression of CD8 $\alpha$  and tdTomato by HR OT-I T cells in liver under control conditions (left) and after DT treatment (right). **b**, Hobit<sup>+</sup> HR OT-I cells were enumerated in control (Ctrl) and DT-treated mice. Two-tailed unpaired *t*-test, \*\**P* = 0.0023, \*\*\**P* = 0.0007. **(c–i)** The contribution of WT and HR OT-I T cells to the formation of primary memory populations was analyzed in control and DT-treated mice. **(c–f)** Representative flow cytometry plots show expression of CD45.1 and CD45.2 to identify the presence of WT (CD45.1<sup>+</sup>) and HR (CD45.2<sup>+</sup>) OT-I T cells within **(c)** CD69<sup>+</sup> T<sub>RM</sub> cells in liver, **(d)** CD69<sup>+</sup> T<sub>RM</sub> cells in SI IEL, **(e)** CD62L<sup>+</sup> T<sub>CM</sub> cells in spleen, and **(f)** KLRG1<sup>+</sup> T<sub>EM</sub> cells in spleen under control conditions (left) and after DT-treatment (right). **(g–i)** The ratio between HR and WT OT-I T cells was determined under control conditions and after DT treatment for **(g)** the CD69<sup>+</sup> T<sub>RM</sub> population of liver and SI IEL, **(h)** the CD62L<sup>+</sup> T<sub>CM</sub> population of spleen and mLN, and **(i)** the KLRG1<sup>+</sup> T<sub>EM</sub> population of spleen and liver. Ratios were normalized to controls. Two-tailed Mann-Whitney *U*-test, \**P* = 0.0286. Data from one experiment (n = 4 mice). Symbols represent individual mice; bars represent the mean.



**Extended Data Fig. 8 | NAD administration results in efficient and selective depletion of WT T<sub>RM</sub> cells.** Wild-type mice containing congenically marked naïve WT and *P2rx7*<sup>-/-</sup> OT-I T cells were infected orally with *L.m.*-OVA. NAD was administered in the memory phase after infection to specifically deplete WT T<sub>RM</sub> cells. After two weeks, presence of donor WT and *P2rx7*<sup>-/-</sup> OT-I T cells, and of host T cell populations was analyzed. **(a–d)** The contribution of WT and *P2rx7*<sup>-/-</sup> OT-I T cells to the formation of primary memory populations was analyzed in control and NAD-treated mice. Representative flow cytometry plots show expression of CD45.1 and CD45.2 to identify the contribution of WT (CD45.1<sup>+</sup>) and *P2rx7*<sup>-/-</sup> (CD45.2<sup>+</sup>) OT-I T cells to the formation of **(a)** CD69<sup>+</sup> T<sub>RM</sub> cells in liver, **(b)** CD69<sup>+</sup> T<sub>RM</sub> cells in SI IEL, **(c)** CD62L<sup>+</sup> OT-I T<sub>CM</sub> cells in spleen, and **(d)** KLRG1<sup>+</sup> T<sub>EM</sub> cells in spleen under control conditions (left) and after NAD-treatment (right). **(e)** Representative flow cytometry plots show expression of Helios and Foxp3 by host CD4<sup>+</sup> T cells in spleen in control (left) and NAD-treated mice (right). **(f, g)** The number of **(f)** Fcpx3<sup>+</sup> Helios<sup>+</sup> CD4<sup>+</sup> T cells and **(g)** TCRγδ<sup>+</sup> T cells in the indicated tissues of control and NAD-treated mice is shown. Two-tailed Mann-Whitney *U*-test. Data is representative of two independent experiments (*n* = 4 mice). Symbols represent individual mice; bars represent the mean.